JTTEE5 25:1088–1110
DOI: 10.1007/s11666-016-0432-6
1059-9630/$19.00 © ASM International

Review

Recent Trends in Newly Developed Plasma-Sprayed and Sintered Coatings for Implant Applications

Suzan Bsat, Andrew Speirs, and Xiao Huang

(Submitted February 22, 2016; in revised form April 25, 2016)

The current paper aims to review recent trends (2011 to 2015) in newly developed plasma-sprayed and sintered coatings for implant applications. Recent developments in plasma-sprayed and sintered coatings have focused on improving biological performance, bacterial growth resistance, and mechanical properties, predominantly of HA and glass ceramics. The majority of these improvements are attributed to the addition of dopants. To improve biological performance, trace elements, such as Zn and Mg, both of which are found in bone, were added to replicate the functions they provide for the skeletal system. Though bacterial growth resistance is traditionally improved by Ag dopant, the addition of new dopants such as CeO_2 and Zn were explored as well. Great effort has also been made to improve coating adherence and reduce stresses by minimizing coefficient of thermal expansion mismatch between the coating and substrate through the addition of elements such as Zn and Mg or the inclusion of a buffer layer. For sintering process in particular, there was an emphasis on reducing sintering temperature through modification of 45S5 Bioglass. New plasma spray and sintering technologies aimed at reducing high-temperature exposure are briefly introduced as well. These include microplasma spray and spark plasma sintering.

Keywords bioactive coatings, biocoating, implant coating, plasma-sprayed coating, sintered coating

1. Introduction

A wide variety of medical conditions are treated with implantable medical devices such as coronary stents, artificial heart valves, total joint replacements, fracture plates, pedicle screws, and soft tissue anchors. These devices typically replace anatomic structures, as is the case with artificial joints, or they augment structures to enable healing of damaged tissues, as is the case with fracture fixation. Development of these devices initially focussed on structural performance, however, in certain cases, as with orthopedic devices, clinical performance relies on integration of the implant into the host bone tissue as well. For example, long-term clinical success of cementless hip implants requires implant stability (Ref 1) which is achieved by the adhesive bonds formed between the bone tissue and the surface of the hip implant (Ref 2). Recognizing the importance of implant-tissue interaction to clinical performance of implants led to the development of implant coatings. In orthopedics, implant coatings are typically applied to improve integration of the coating through adhesive bonding with bone tissue, known as osseointegration (Ref 2, 3). In developing these coatings, the ability to rapidly form strong adhesive bonds with bone tissue is a main concern in providing stability, while mechanical integrity is equally as important for clinical success.

Although implant coatings have been in use for decades, new and enhanced implant coatings are continuously being developed with a focus on improving mechanical properties and biological behaviour. These coatings with bioactive surface and adequate mechanical strength may be produced by a variety of technologies, two of which include plasma spray and sintering. The purpose of this review is to discuss recent trends (2011 to 2015) in newly developed plasma-sprayed and sintered coatings for implant applications. While implant coatings have also been developed to elute specific drugs or growth factors into the surrounding tissues, such applications are beyond the scope of this review. With implant adhesion being a main concern in developing implant coatings, a brief introduction to implant adhesion is provided.

2. Introduction to Implant Adhesion

Bone tissue consists of two phases: an organic collagen-rich osteoid phase synthesized by osteoblast cells, and a mineral phase of calcium-deficient carbonated apatite (Ref 2) with similar composition to hydroxyapatite (HA: $Ca_{10}(PO4)_6(OH)_2$). Upon insertion of an implant, new bone formation occurs by osteoid synthesis and mineralization, and adhesion is achieved by mechanical interlock

Suzan Bsat, Andrew Speirs, and **Xiao Huang**, Carleton University, Ottawa, ON K1S5B6, Canada. Contact e-mail: suzanbsat@cmail.carleton.ca.

Table 1 Influence of relative motions at the implant-bone interface on bone ingrowth into porous implants (Ref 7)

Interface micromotions (μm)	Tissue response
0 to 20	Bone ingrowth and secure fixation of implant to host bone tissue
>40	Bone formation within implant pores, but not connected to host bone tissue (i.e., loose)
>150	Implant connected to bone through fibrous tissue layer

Table 2 Simulated body fluid (SBF) with pH 7.4 at 36.5 °C which mimics blood plasma (Ref 9)

Component	Concentration (mM)
Na^+	142.0
K^+	5.0
Mg^{2+}	1.5
Ca^{2+}	2.5
Cl^-	147.8
HCO_3^-	4.2
HPO_4^{2-}	1.0
SO_4^{2-}	0.5

with surface pores and/or chemical bonding with the implant surface.

Implant surfaces may be classified as osseoinductive, which promote osseogenesis (the formation of bone) and thereby form a chemical bond to bone; or osseoconductive, which simply allow the growth of bone over the surface and typically achieve stable fixation through mechanical interlock of tissue with surface porosity or roughness. Bone-to-implant adhesion is affected by many factors such as relative movement between the implant and bone, surface roughness or porosity, and surface chemistry. Table 1 explains how bone ingrowth is affected by relative motion between the implant and bone, where motion greater than 40 μm results in loose implant fixation. For porous bioinert implant surfaces which require mechanical interlock, direct bone ingrowth can occur when pore sizes are at least 75 μm, but ideally greater than 100 μm, which allows penetration of blood vessels to maintain the living bone tissue (Ref 4). While fibrous, noncalcified tissue may form in smaller pores (Ref 4), fibrous tissue around an implant is associated with implant loosening (Ref 5). See Oliveira et al. (Ref 6) for a review of the influence of surface porosity, material, and interface conditions on bone ingrowth.

The surface chemistry of the implant coating also plays a significant role in implant adhesion. The surface chemistry is a main factor in determining its bioactivity, assessed by its ability to promote HA formation. The initial formation of HA is often recognized as an early predictor to bone formation. HA forming ability is assessed by immersing a component in simulated body fluid (SBF, Table 2) followed by measurement of the surface phases by x-ray diffraction (Ref 3) or x-ray photoelectron spectrometry (Ref 8).

Various coating compositions have been explored to find optimal surface chemistry for HA formation. It has been shown that terminal functional groups (i.e., ligands exposed at the surface) PO_4H_2, COOH, $CONH_2$, OH, and NH_2 on alkanethiols have apatite forming ability, with the PO_4H_2 and COOH inducing the highest HA formation rate and much lower growth rates for $CONH_2$ and OH (Ref 8). This HA forming ability of a surface is known as bioactivity and is due to the negative surface charge of PO_4H_2 and COOH binding Ca^{2+} ions which could then complex with phosphate ions to form HA. The other groups involved ion-dipole interactions or would weakly bind phosphate which seemed less favorable for HA growth. Viitala et al. (Ref 10) showed that HA nucleation begins with Ca^{2+} binding to negative surface charges, which is dependent on surface chemistry. However, HA growth is dependent on surface topography as well. Thus, various studies focus on modifying surface chemistry/topography to achieve desirable bioactivity of surface coatings.

3. Plasma Spray

Plasma spraying is the most commercially used process in applying metal or ceramic coatings to orthopedic or dental implants (Ref 11). Plasma spraying is particularly advantageous to industry because of its fast deposition rate (Ref 12). The technique involves melting a stream of powder particles in a high-temperature plasma flame as they are discharged toward the implant surface.

This section reviews recent efforts made toward developing new or enhancing existing plasma-sprayed biocoatings, particularly HA and glass ceramic coatings.

3.1 Hydroxyapatite Coatings

HA is arguably one of the most studied coatings for implant applications and is most commonly deposited using plasma spraying technique (Ref 13). HA is a calcium phosphate bioceramic with stoichiometric form $Ca_{10}(PO_4)_6(OH)_2$, similar to that of human bone mineral components (Ref 2). With its similar chemical composition, the bioceramic is widely studied because of its osseoconductive nature which functions to enhance bone-implant interaction by stimulating bone growth and osseointegration. Although studies of HA date back several decades and the coating is used commercially today, recent literature continues to have significant content relating to the development and evolvement of HA coatings. Studies have focused on improving mechanical properties, biocompatibility and bioactivity, and resistance to bacterial growth as they are critical for long-term implant applications (Ref 13-15).

The addition of silicon-containing compounds to HA coatings has been explored to enhance biocoating prop-

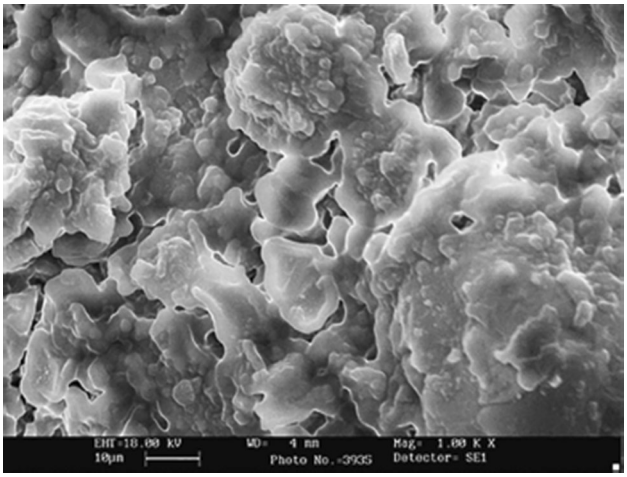

Fig. 1 SEM micrograph of 10 wt.% zircon in HA (Reprinted from Ref 13, Copyright (2014), with permission from Elsevier)

erties. The choice of silicon is based on its known role in the bone remodeling process and in maintaining healthy bone. Given its role, the addition of silicon is expected to help with the growth, proliferation, and differentiation of osteoblast cells for new bone formation (Ref 16, 17), ultimately increasing the bioactivity and osseointegrative nature of the implant surface. In fact, previous studies have shown that silicon-modified HA results in increased negative surface charge attributed to the van der Waals effect of the more easily polarized Si atom (Ref 18), with Si substituting for P in the PO_4^{3-} ion (Ref 19). The increased negative surface charge would tend to promote bone growth by attracting calcium ions which then bind to phosphates in the process of bone growth (Ref 18). The fact that negatively charged surfaces and Si-HA in particular are highly conducive to bone growth has been shown empirically both in vitro (Ref 19-21) and in vivo (Ref 19, 22). Diatomaceous earth (DE) as a source of silicon has also been demonstrated to result in improved bioactivity of Si-HA relative to the use of silicon from pure silica, possibly owing to the trace amounts minority elements Na, Mg, Al, K, and Fe in DE (Ref 23, 24) allowing it to more closely mimic natural bone in terms of composition (Ref 22). For these reasons, recent literature has continued to explore the addition of silicon to HA coatings.

Karamian et al. (Ref 13) modified HA coating through the addition of zircon ($ZrSiO_4$) to improve the biological characteristics of HA. HA/zircon nano-biocomposite coatings with 0, 5, 10, and 15 wt.% zircon were deposited onto 316L SS dental implants (Fig. 1) and immersed in SBF. The thickness of HA layer after SBF immersion increased with increasing zircon content up to a maximum of 10 wt.%. 10 wt.% zircon had the highest release of Ca^{2+} and PO_4^{3-} ions leading to local supersaturation required for nucleation and growth of apatite (Ref 25). It was hypothesized that HA/zircon coatings were superior to HA alone because of the silicate ions released. While the introduction of Si through zircon proved to enhance bioactivity of HA, in a separate study the addition of SiO_2 (1, 2 and 5 wt.%) had no effect on bioactivity or mechanical properties (Ref 26).

While HA alone has been of particular interest because of its compositional similarity to natural bone, natural bone mineral is also composed of doped ions such as Sr^{2+} (Ref 27), Mg^{2+} (Ref 28), CO_3^{2-} (Ref 29), and F^- (Ref 30). These ions, as in the case of Si, have important functions to the skeletal system (Ref 31, 32), therefore to improve bioactivity of HA coatings ion-doped HA coatings have been recently developed. Strontium in particular has the ability to stimulate collagenous and noncollagenous protein synthesis and block osteoclastic bone resorption without cytotoxic effect on osteoblasts (Ref 33-35). Li et al. (Ref 36) have shown that plasma-sprayed Sr-doped HA had a positive effect on proliferation of osteoblast-like cells as compared to HA alone (Fig. 2) while also maintaining HA formation.

Apart from improving bioactivity of HA, efforts to improve mechanical properties have also been a focus in enhancing HA further. Al_2O_3-13 vol.% TiO_2 (AT13) was deposited with HA in a bilayer manner on CP-Ti dental implant material to improve wear resistance while maintaining bioactivity through HA (Fig. 3) (Ref 37). AT13 has been previously used to coat titanium implant surface and was shown to have superior wear resistance and adhesive strength (Ref 38). It has therefore been deposited with HA, to compensate for the poor mechanical properties of HA. Bilayer coating improved wear resistance and hardness as compared to HA and AT coatings applied separately. Titanium alloy Ti-24Nb-4Zr-7.9Sn has also been combined with HA to achieve ideal coating mechanical properties while maintaining bioactivity (Ref 39). Ti-24Nb-4Zr-7.9Sn in particular comes from a series of Ti alloys which have been specifically developed to have low elastic modulus while maintaining satisfactory strength. An increase in Ti alloy content (80 wt.% in a mixture of Ti alloy/HA) resulted in improved mechanical properties, while the opposite was observed for bioactivity. Singh et al. (Ref 40) combined HA and CaP in a coating, as both have given superior bioactivity in clinical trials. However, the corrosion resistance tests of HA and HA-CaP coatings in SBF showed that HA coating deposited onto 316 L stainless steel substrate has superior corrosion resistance as compared to HA-CaP composite coating. Furthermore, following the corrosion test surface morphology of HA was unchanged while those with HA-CaP lost their surface roughness, due to the corrosion process. While CaP may improve bioactivity, its poor corrosion resistance can degrade long-term success and mechanical properties of the implants. Furthermore, high levels of released ions from corrosion products of HA-CaP may cause adverse reaction to the body.

Recently trending among biocoating literature is the incorporation and enhancement of bacterial growth resistance, particularly through the addition of silver. Prosthetic joint infection can complicate and prolong treatment following the insertion of prosthetic joints (Ref 41). It is caused by bacteria adhering and growing on implanted joints, however may be avoided by enhancing

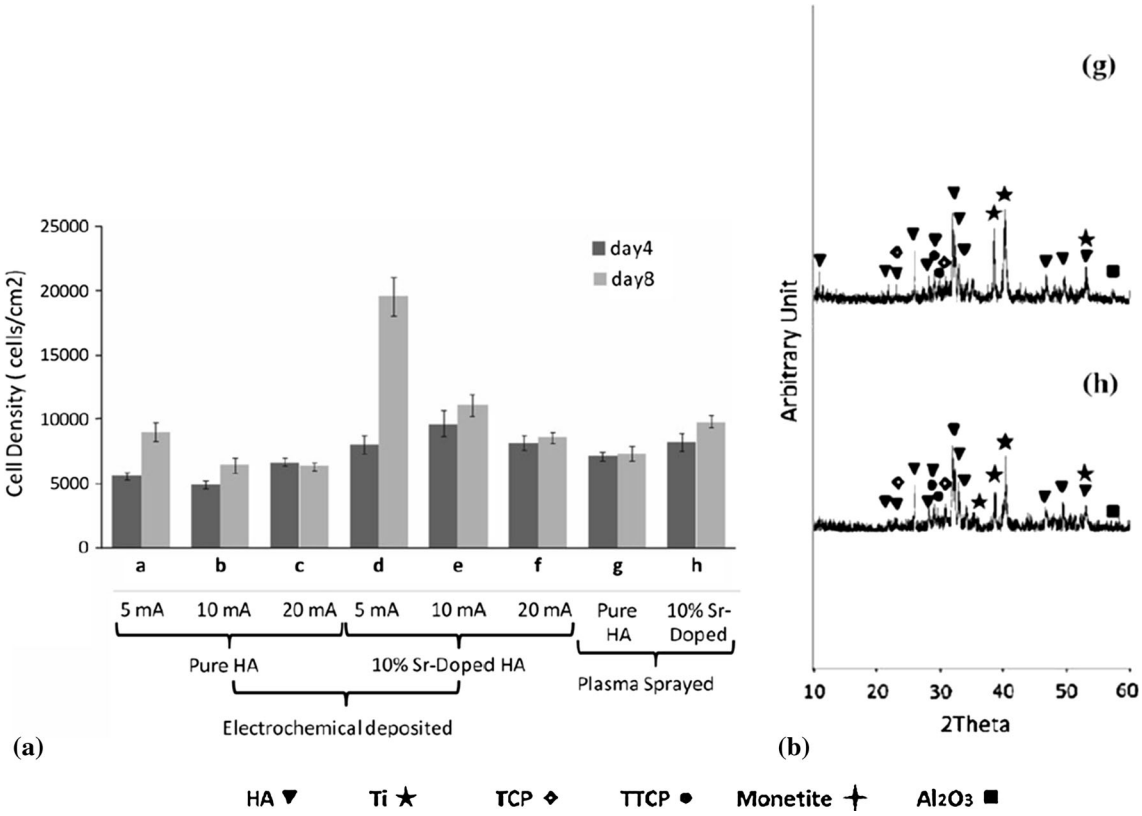

Fig. 2 (a) Cell culture results of HA (g) and Sr-doped HA (h) and (b) x-ray diffraction spectra post-SBF immersion (Reprinted from Ref 36, Copyright (2012), with permission of Springer)

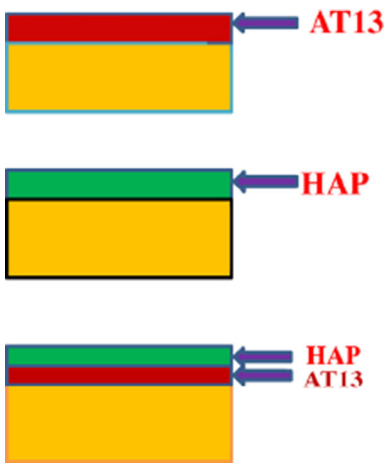

Fig. 3 Bilayer HA and AT (Reprinted from Ref 37, Copyright (2014), with permission from Elsevier)

bacterial resistance. The addition of silver imparts antibacterial properties to implants as it is able to help prevent infections. Studies have shown that Ag^{+} can penetrate through bacterial cell walls and can condense DNA such that it reacts with the thiol group proteins to cause cell death (Ref 42). In terms of its use with HA coatings, Roy et al. (Ref 14) found that optimum amount of silver oxide (Ag_2O) was between 2 and 4 wt.% (Fig. 4) which had excellent antimicrobial property without altering the mechanical properties.

Fielding et al. (Ref 15) studied the incorporation of both Ag_2O and SrO (strontium oxide) into HA for improved antimicrobial activity and cell material interactions, respectively. Sr is able to displace Ca^{2+} ions in osteoblastic calcium-mediated processes and thus stimulate bone formation by activating calcium sensing receptors (Ref 43, 44) while also inhibiting bone resorption (Ref 45). 1 wt.% SrO/2 wt.% Ag_2O-HA coatings were prepared using plasma spray equipped with supersonic plasma nozzle (Ref 15). The addition of silver alone was highly effective against bacterial colonization; however, cytotoxic effects were evident as characterized by poor cellular morphology and cell death. However, through the addition of SrO these effects were offset and improved performance of cell viability was observed as compared to HA alone. The addition of dopants also enhanced bonding strength.

Alternatively, rather than modifying HA powder to enhance the HA coating, studies have also focused on treating the substrate surface prior to plasma spraying to improve coating properties. While surface chemistry is critical for the bioactivity of the implant surface, surface topography is equally important. Developed morphological heterogeneity (on a nanometer scale) and nano-sized

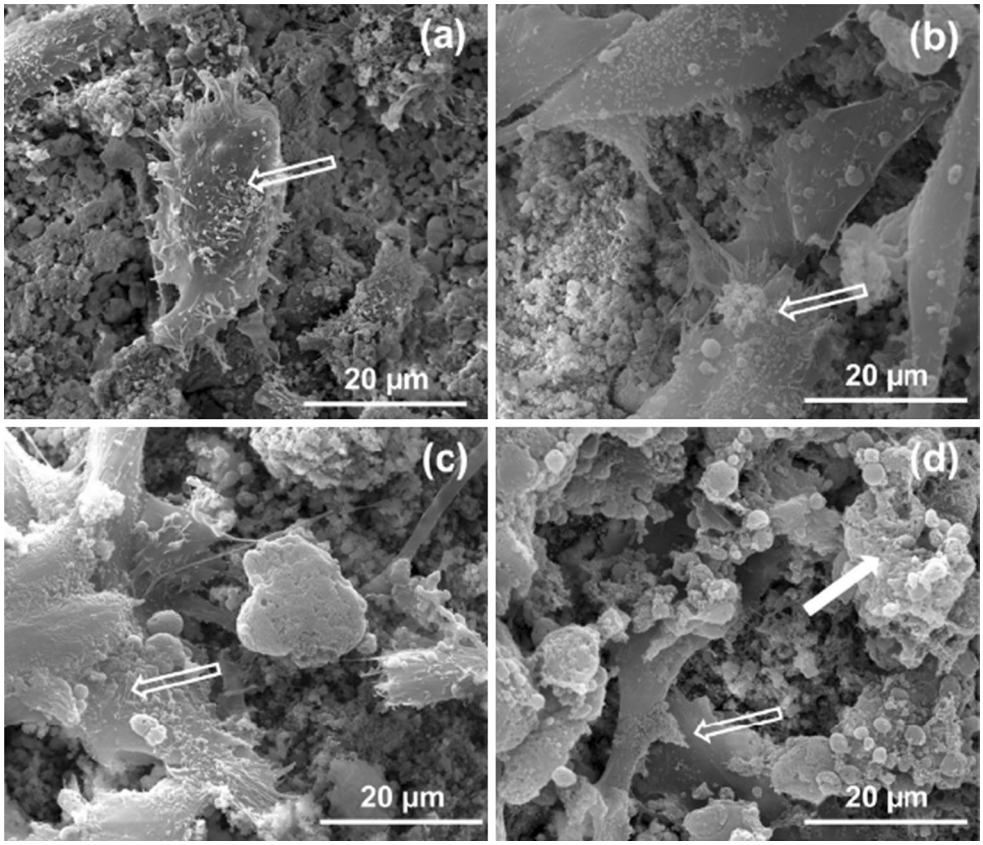

Fig. 4 SEM micrograph of (a) 0 wt.% Ag, (b) 2 wt.% Ag, (c) 4 wt.% Ag, and (d) 6 wt.% Ag. Open arrow indicates live cell, closed arrow indicates dead cell (Reprinted with permission from Ref 14, Copyright (2012) American Chemical Society)

grains impact implant-bone interactions. Previous studies have shown that the presence of nano-topographical features helps promote the initial formation of Ca and P, and later apatite or bone (Ref 46-48). The natural human extracellular matrix is a complex network made up of a collection of nano-scale structures and features and hence is stimulated and interacts with cells on a nano-scale level (Ref 49-51). For bone, the use of artificial nano-structures allows intimate interactions with the first level of bone structural hierarchy allowing repopulation and re-synthesis of a new matrix for bone. To obtain morphological heterogeneity on a nano-scale, induction heat treatment (IHT) of substrates prior to plasma spray deposition was used (Ref 52). HA was plasma-sprayed on titanium alloy substrates subjected to IHT from 20 to 1000 °C. It was shown that both morphology and grain size could be controlled based on the temperature used for IHT before spraying. For temperatures between 800 and 1000 °C, separate agglomerated particles 30 to 90 nm in size and an average grain size of 6 nm were observed. In a separate study, it was shown that heat treatment of Ti-6Al-4V substrate to 250 °C prior to plasma spraying SiO_2-doped HA (1, 2 and 5 wt.%) significantly improved the mechanical properties of the coating as compared to pure HA (Ref 26). Without preheat treatment of substrates, the SiO_2 had no added effect on the mechanical properties of the coating. The authors attribute this finding to the highly porous microstructure with low crystallinity in SiO_2-doped HA coatings without preheat treatment.

3.2 Titania Coatings

While HA is arguably the main focus of biocoating research, titania (TiO_2) has received some attention as well. As compared with TiO_2, HA has lower tensile and shear strengths and, although results can vary with the raw materials and processes used, in general, its interfacial bond strength to a titanium substrate is no better than plasma-sprayed porous TiO_2 coatings. Furthermore, in certain forms HA may be resorbable, whereas resorption is not a concern with TiO_2. HA is primarily superior to TiO_2 in its osseointegration. The osseoinductivity of the HA coating does lead to high early fixation strength but studies suggest that the long-term performance is different from plasma-sprayed porous TiO_2 coatings (Ref 53-55) with one study finding that at 6 months postsurgery, 50 to 75% more bone surrounded titanium controls than the HA-coated implants (Ref 56). For these reasons, recent studies have continued to explore the use of TiO_2 coatings.

In an effort to improve the mechanical properties and bioactivity of TiO_2 coating, ZrO_2 was added because of its mechanical strength (Ref 57) and favorable biocompatibility and osteogenic properties (Ref 58-61). 30 wt.% ZrO_2/TiO_2 composite coating was plasma-sprayed onto Ti plates, as shown in Fig. 5 (Ref 62). The shear bond strength was higher, and enhanced biological behaviour of human bone marrow mesenchymal stem cells was observed in ZrO_2/TiO_2 coatings as compared to TiO_2 alone.

Most recently cerium oxide (CeO_2)-doped TiO_2 coating on commercially pure (CP)-Ti substrate was developed to enhance antibacterial property as well as microstructure (Ref 63). Ceria has been shown previously to have excellent antibacterial properties (Ref 64, 65) while having no effect on bioactivity (Ref 64). The addition of CeO_2 improved corrosion resistance and antibacterial properties and had no adverse effect on osteoblast cells. The CeO_2 did not significantly change the rutile structure of TiO_2, and 10 wt.% CeO_2 was found to have the highest activity against bacteria (Fig. 6).

3.3 Other Coatings

Ceramics have been widely used as biomaterials in medicine, mainly for their wear and corrosion resistance as well as biocompatibility (Ref 66, 67). Sathish et al. (Ref 68) prepared ceramic bilayer coating similar to that shown in Fig. 3. AT13 was combined in a bilayer manner with yttria-stabilized zirconia (YSZ) by plasma spraying onto a preheated (400 °C) Ti-13Nb-13Zr alloy to improve wear and corrosion. Corrosion and wear resistance were substantially improved in the bilayer coating as compared to either coating alone. Similarly, Yildiz et al. (Ref 69) applied alumina ceramic coating to 316 L stainless steel

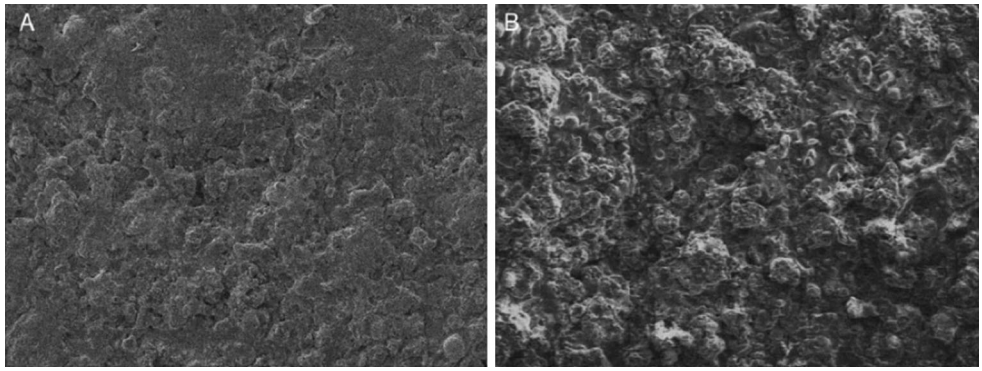

Fig. 5 SEM micrograph of (a) TiO_2 and (b) 30 wt.% ZrO_2/TiO_2 (Ref 62, by permission of Oxford University Press)

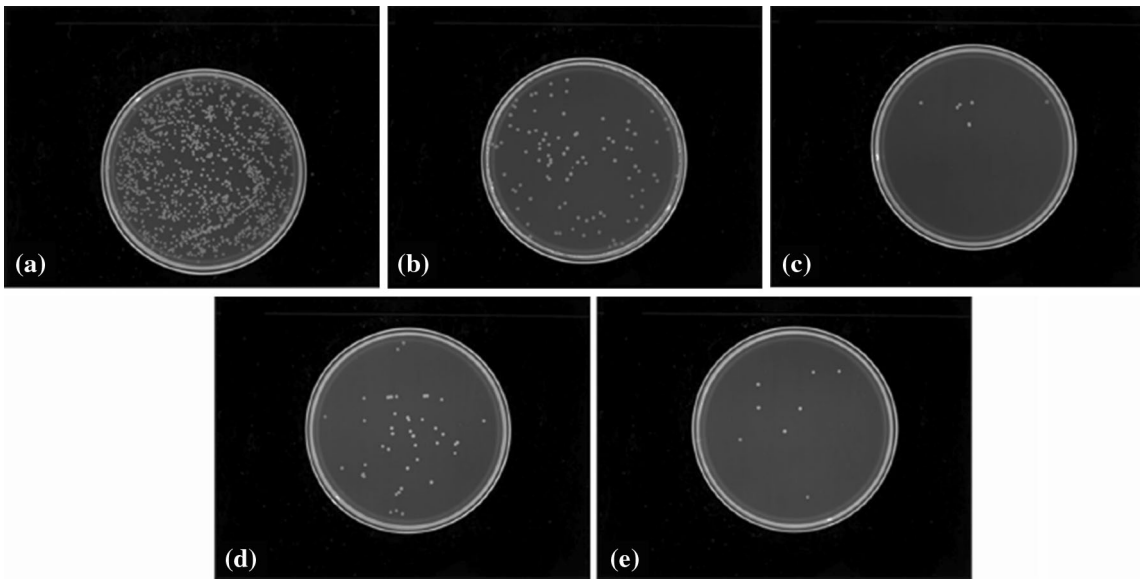

Fig. 6 Recultivated bacterial colonies on agar: S. aureus colonies are previously dissociated from (a) TiO_2, (b) 5%CeO_2/TiO_2, (c) 10%CeO_2/TiO_2, (d) 20%CeO_2/TiO_2, and (e) CeO_2 coatings after 24 h incubation (Reprinted from Ref 63, Copyright (2015), with permission of Springer)

implant to improve wear and corrosion resistance in SBF, both of which were achieved. The arc current (300 versus 500 A) was found to have no effect on wear resistance and corrosion resistance but contributed to an increased surface roughness. Alumina has also been deposited on implant surface as a buffer layer between the Ti-6Al-4V implant and HA outer layer for the purpose of depositing a coating with similar coefficient of thermal expansion (CTE) as the substrate (Ref 70), in an attempt to reduce thermal stresses at the coating-substrate interface. The alumina also acts as a diffusion barrier to prevent Al and V being released into the body, both of which are associated with health risks (Ref 71, 72). A thin layer of HA is then deposited on top of the alumina by dip coating method to provide bioactivity for early mineralization. It is expected that with time HA dissolution will occur as has been previously observed (Ref 53); however, the underneath bioinert alumina coating will remain.

3.4 Plasma Spraying Parameters

In terms of plasma spraying HA, finding the most ideal parameters for coating deposition remains a challenge. Hung et al. (Ref 73) varied parameters to determine those ideal for spraying HA on titanium alloy (Ti-6Al-4V) dental implants measuring 4.5 mm in diameter. The range of current for typical plasma-sprayed HA coating is ~350 to 1000 A (Ref 74), which is proportional to the power. It has been shown that high-power plasma spraying can elevate flame temperature and improve particle melting as well as increase particle speed (Ref 75, 76). However, increased current or power in HA coatings leads to a decrease in degree of crystallization on HA coatings (Ref 74, 77, 78). Spraying distance has also been investigated, and it has been found that with increasing spray distance crystallization is reduced, porosity is increased, fractures are increased (Ref 78), and mechanical properties are reduced (Ref 79). Hung et al. (Ref 73) found that optimal mechanical properties were obtained at 10 cm. For rod-shaped and dental screw-shaped implants, b1 and c1 spray parameters (Fig. 7), respectively, achieved best coating in terms of thickness, crystallinity, composition, and adhesion strength.

Evidently, plasma spray parameters strongly affect the resulting mechanical properties. As discussed by Gross et al. (Ref 80), establishing distinct properties of plasma-sprayed HA coatings is difficult as manufacturers and suppliers all use different processing conditions leading to a high variability in mechanical properties. This variability has been reported for coatings with crystalline structure but is not present for those with amorphous phases. Using nanoindentation techniques, the hardness and elastic modulus of amorphous and crystalline phases were measured on HA coatings deposited on a collection of implants obtained from different manufacturers (Ref 80). Amorphous phase had average hardness of 1.5 ± 0.3 GPa and elastic modulus of 48 ± 6 GPa. Crystalline regions had hardness between 3 and 7 GPa, with the higher values residing with sintered crystalline HA. The lower values were found to be attributed to cracking in the coating and the presence of amorphous areas. Overall hardness varied between 1 and 8 GPa. The use of nanoindentation was proven to be useful in producing a mechanical property map as small regions are accessible.

Based on the variability in mechanical properties reported above, standard parameters for HA-based coatings have not been established. As such, Table 3 condenses some plasma spraying parameters recently used in literature when preparing HA-based coatings. They may serve as initial spraying parameters if similar coatings are to be prepared for future studies. Parameters for some glass ceramic coatings are included as well.

3.5 Glass Coatings

In place of using HA as an implant coating, glass ceramics have also been applied. Most recently calcium-silicate ($CaSiO_3$) ceramic glass systems have been modified to improve their chemical stability, bioactivity, and mechanical integrity. Although $CaSiO_3$ systems have been used to enhance bioactivity (Ref 81), some limitations exist. Calcium-silicate ceramics have been found to have high dissolution rates (Ref 82), with high ionic dissolution of $CaSiO_3$ potentially leading to high-local pH environment which can result in adverse cellular response

Exp no.	a1	a2	a3	a4	a5	a6	b1	c1
Flow rate of primary gas (Ar) (l/min)	50	50	50	50	50	50	50	50
Flow rate of secondary gas (H_2) (l/min)	14	6	0	14	6	0	14	14
Surface speed (Vs, rpm)	150	150	150	150	150	150	150	5
Transverse speed (Vt, mm/s)	5	5	5	5	5	5	5	400
Flow rate of powder carrier gas (Ar) (l/min)	3	3	3	3	3	3	3	3
Powder feed rate (rpm)	10	10	10	27	27	27	10	10

Fig. 7 Optimal parameters for plasma spraying HA on rod-shaped (b1) and dental screw-shaped (c1) implants (Reprinted from Ref 73, Copyright (2013), with permission from Elsevier)

Table 3 Atmospheric plasma spray parameters for HA and glass ceramic coatings

Author	Powder spray distance (mm)	Flow rate Ar carrier gas (slpm)	Power (kW)	Spray voltage (V)	Spray current (A)	Flow rate primary/secondary/sheath gas (slpm)	Powder feed rate (g/min)
APS HA coatings							
Xu et al. (Ref 26)	HA; SiO_2 doped HA90	3	…	…	600	40 (Ar)/20 (He)/…	…
Karamian et al. (Ref 13)	HA; HA/zircon…	23.6	…	50	500	56.64/…/…	…
Yi et al. (Ref 96)	HA300	3.5	…	65	650	40 (Ar)/10 (H_2)/…	26
APS ceramic coatings							
Wang et al. (Ref 88)	hardystonite ($Ca_2ZnSi_2O_7$); sphene ($CaTiSiO_5$)100	3.5	…	70	600	40 (Ar)/12 (H_2)/…	20
Maleki-Ghaleh et al. (Ref 91)	Merwinite ($Ca_3Mg(SiO_4)_2$)100	10	…	55	400	85 (Ar)/10 (H_2)/…	9
Yi et al. (Ref 96)	Bredigite($Ca_7MgSi_4O_{16}$)120	3.5	…	66	600	40 (Ar)/10 (H_2)/…	26
Zhao et al. (Ref 63)	CeO_2 doped $TiO_2$100	…	40	…	…	40 (Ar)/12 (H_2)/…	30
Si et al. (Ref 62)	ZrO_2 doped $TiO_2$80	…	40	…	…	50 (Ar)/6 (H_2)/…	30
Khalid et al. (Ref 70)	$Al_2O_3$130	11.8 (N_2)	…	70	504	79 (Ar)/4.7 (H_2)/…	22.7

(Ref 83, 84). Yu et al. (Ref 82) added Zn to improve chemical stability (solubility), and bioactivity of calcium-silicate ceramic coatings as zinc is known to stimulate bone formation while inhibiting osteoclastic bone resorption (Ref 85). A lack of zinc has been shown to impede the growth, development, and maintenance of bone (Ref 86, 87). Hardystonite ($Ca_2ZnSi_2O_7$) was therefore plasma-sprayed onto Ti-6Al-4V. The added zinc enhanced cell attachment, proliferation, and differentiation as compared to $CaSiO_3$ coatings and uncoated Ti alloy. In a rabbit femur model, the added zinc also demonstrated new bone formation in direct contact with the coating. Wang et al. (Ref 88) also explored hardystonite ($Ca_2ZnSi_2O_7$) in addition to sphene ($CaTiSiO_5$). Both powders with nano-structures were deposited by plasma spray on Ti-6Al-4V discs. Both had bonding strength greater than that reported for HA. Primary human osteoblasts attached, spread, and proliferated well on both types of coatings because of the Ca and Si ions released. The addition of controlled release of Ca and Si ions has been shown to enhance osteoblast attachment, proliferation, and differentiation (Ref 84, 89, 90). Cell attachment and proliferation however were higher for hardystonite coatings as a result on Zn ions. The addition of ZnO and TiO_2 into the $CaSiO_3$ system also resulted in better chemical stability and reduced difference in CTE between coating and substrate. Matching coating-substrate CTE is important in avoiding high thermal stresses at the coating-substrate interface.

The addition of magnesium to $CaSiO_3$ system has also been developed to enhance chemical stability (Ref 91). Merwinite, a tricalcium magnesium silicate powder ($Ca_3Mg(SiO_4)_2$), deposited on magnesium alloy has been shown to enhance chemical stability and increase bioactivity (Ref 92, 93). $Ca_3Mg(SiO_4)_2$ was therefore deposited on Ti-6Al-4V alloys using plasma spray technique. Chemical stability as well as distribution and proliferation of cells was improved as compared to the bare counterparts. Also the CTE of $Ca_3Mg(SiO_4)_2$ (9.87×10^{-6}/ °C) is close to that of Ti-6Al-4V (9.80×10^{-6}/ °C) (Ref 94) as compared to HA (11.5×10^{-6}/ °C) (Ref 95). Bredigite coating, another $CaSiO_3$ coating infiltrated with Mg ($Ca_7MgSi_4O_{16}$), was prepared on Ti-6Al-4V substrate using plasma spraying technique (Ref 96). Bonding strength reached 49.8 MPa, significantly higher than HA and other silicate-based bioceramics prepared by atmospheric plasma spray (APS). A distinct apatite layer was observed following SBF immersion and enhanced attachment and proliferation of rabbit bone marrow stem cells was observed as compared to HA. The authors suggest that the released SiO_4^{4-} and Mg^{2+} ions and the formed nano-apatite layers are what contributed to cell proliferation.

Another variation of the calcium-silicate system, namely P_2O_5-Na_2O-CaO-SiO_2, has been shown to synthesize nano-structured coatings through liquid plasma spraying process, where a suspension is used as the feedstock (Ref 97). Quick formation of nano-structured hydroxyl carbonate apatite (HCA) layer following SBF immersion was observed. The authors use the formation of

HCA as an indicator for bioactivity as its formation speed has been associated with early bone ingrowth rate and new bone formation (Ref 98).

3.6 Alternatives to Atmospheric Plasma Spray (APS)

Alternative plasma spray technologies may provide enhanced structural morphologies and compositions to enhance coatings, HA in particular. The high-temperature plasma jet in APS induces undesirable phase changes of HA resulting in powder decomposition and formation of a mixture of amorphous calcium phosphate (ACP), tricalcium phosphate (TCP), tetracalcium phosphate (TTCP), calcium oxide (CaO), and dihydroxylation products (Ref 99). CaO is particularly harmful as a hydration reaction occurs during storage or after implantation in vivo where CaO transforms into $Ca(OH)_2$ with a 50% volume increase, resulting in internal strains and cracks (Ref 100). Furthermore, phases such as TTCP or CaO do not have any proven bioactivity and dissolve faster than other calcium phosphate phases. Dissolution rates of other phases formed during spraying follow the order ACP $\gg$ TTCP $\gg$ α-TCP $\gg$ OHA $\gg$ β-TCP $\gg$ HA (Fig. 8) (Ref 101, 102). While partial dissolution of HA coating is necessary for biological bonding, excessive dissolution can result in implant loosening as a result of excessive coating disintegration (Ref 53). For example, while HA can maintain its phase stability up to 1200 °C, it will transform into TCP at higher temperatures which is highly soluble in the body environment and can result in decreased implant stability (Ref 103). Optimum phase of HA is still debated as crystalline HA has been shown to be crucial for in vivo stability (Ref 104, 105) while soluble amorphous calcium phosphate (ACP), ATP, TTCP has found to accelerate bone attachment rate but may also be detrimental if excessive (Ref 106).

To eradicate issues surrounding high-temperature plasma, microplasma spraying (MPS) may be used in place of conventional plasma spraying to enhance HA coatings. MPS is characterized by low plasma power (1 to 4 kW), low plasma gas flow rate, and low heat input into the substrate (Ref 107). MPS is particularly useful for the application of coatings on small parts or with high accuracy because of its smaller spray spots (3 to 5 mm) due to its narrow laminar plasma jet. These properties are very advantageous for the application of HA coatings as the temperature of the plasma jet is considerably lower than conventional plasma spraying. It generally avoids formation of impure amorphous phases, provides a higher degree of purity and crystallinity and a higher degree of porosity to facilitate bone ingrowth (Ref 107). MPS has been shown to achieve ~92% crystalline HA coatings (Ref 108) while APS is between 65 and 80% (Ref 109, 110). Furthermore, low thermal input of MPS allows 250 μm thickness with 20% porosity without affecting material properties (Ref 106). APS HA is limited to ~150 μm thickness due to accumulation of residual stress (Ref 111) and are highly dense (2 to 10% porosity). Though APS is still primarily used, experimentation with MPS is visible among the literature.

Dey et al. (Ref 112) have used MPS to evaluate HA and β-TCP-coated 316L SS pin for intra-medullary bone repair in a rabbit model. Performance of MPS β-TCP-coated pins was better than HA coated and uncoated pins in terms of new bone formation and apposition. Also the bone defect healing was better presumably due to better bone bonding and osseointegration in β-TCP-coated pins. MPS has also been used to deposit HA on 316L SS strips where 200 μm thickness and 11 vol.% porosity was attained (Ref 113). Microcracks were observed likely due to thermal shock or mismatch in CTE. Toughness value of 0.59 MPa $m^{1/2}$ at 100 mN load was found, higher than that reported for APS HA (Table 4). An SBF immersion study was also conducted on the samples where needle-like nano-structured apatite was observed on the surface after 4 to 14 days immersion (Ref 107).

Similarly, low-energy plasma spray (LEPS), an experimental low-energy version of a conventional plasma spray system has been used to deposit osteoconductive coatings on small-sized bone implants (Ref 99). Use of conventional APS to coat small implants (e.g., dental implants) produces irregular nonoptimal coatings, with concerns of failure due to microbiological susceptibility, resorption, and interfacial fracture-risk issues. Furthermore, for threaded designs, thin, controlled, and homogenous coatings are challenged by APS. This gives need for LEPS mini-gun to coat small, geometrically complex implants. Demnati et al. (Ref 115) developed a portable LEPS system for deposition of HA coatings on small-sized implants with complex geometry. Using LEPS phase purity and crystallinity of HA are better than those reported for APS without posttreatment.

Most recently, LEPS has been used to deposit HA/PCL (0.5 to 1.3 wt.%) composite coating onto Ti metallic components for femoral stem or dental implant applications (Ref 99). PCL is a polymer (poly-ε-caprolactone) with high toughness at body temperature and does not produce an acidic environment during degradation. Adding bioresorbable polymer as a second phase favors the release of residual stresses in HA coatings allowing for the production of thick coatings. Furthermore, they can encapsulate drugs for in situ drug release. To avoid degradation of the polymer, LEPS was used, with both components injected into different zones of the plasma plume. LEPS successfully deposited HA/PCL biocoatings without major PCL degradation. PCL improved layer thickness per spray pass which has economic impact, gave higher porosity with same mechanical properties as HA alone, and had higher surface roughness. Attachment and proliferation of murine osteoblast-like cells was confirmed.

While LEPS can be used to deposit polymer, Wolinne et al. (Ref 116) used a vacuum plasma spray (VPS) process to deposit metal coatings onto high- and low-temperature melting polymers including PEEK and polyethylene. VPS is performed in an Ar atmosphere at low pressure (1 to 600 mbar) with power between 5 and 30 kW. Using VPS, titanium coating was deposited on medical grade polyethylene. VPS did not cause substantial degradation but induced melting and recrystallization of

Phase	Chemical Formula	Abbreviation	Solubility Constant Ks at 25°C[69]	Crystal Structure/References	JCPDS No.
Hydroxyapatite	$Ca_{10}(PO_4)_6(OH)_2$	HA	6.62×10^{-126}	Hexagonal $P6_3/65$	9-432
Amorphous phase	N/A	ACP	N/A	Irregular	N/A
Alpha tricalcium phosphate	α-$Ca_3(PO_4)_2$	α-TCP	8.46×10^{-32}	Monoclinic $P2_1/a/66$	9-348
Beta tricalcium phosphate	β-$Ca_3(PO_4)_2$	β-TCP	2.07×10^{-33}	Rhombohedral R3c/67	9-169
Tetracalcium phosphate	$Ca_4P_2O_9$	TTCP	N/A	Monoclinic $P2_1/68$	25-1137
Oxyhydroxyapatite	$Ca_{10}(PO_4)_6(OH)_{2-2x}(O)_x(\square)_x$	OHA	$\sim 10^{-69}$ (oxyapatite)	Hexagonal/62 $P6_3/62$	9-432

Fig. 8 Calcium phosphate phases in HA coatings (Ref 53, Copyright © 2001 by John Wiley Sons, Inc. Reprinted by permission of John Wiley & Sons, Inc.)

Table 4 Toughness of HA prepared by APS and MPS (Ref 108, 114)

Process	Fracture toughness (MPa $m^{1/2}$)
APS	0.39 to 0.55
Bulk	1
MPS	0.6

polyethylene near the interface. For small displacements (<1.2 mm), coated samples were substantially stiffer, while larger displacements resulted in similar stiffness to the uncoated control (Fig. 9).

As opposed to MPS or LEPS, gas tunnel-type plasma spray characterized by its high-power plasma jet, successfully deposited YSZ (10, 20, and 30 wt.%)-reinforced HA coatings (Ref 117). The gas tunnel YSZ enhanced both hardness, wear resistance, and adhesive strength of the coatings while also exhibiting superior corrosion resistance as compared to HA alone. Furthermore, SBF testing showed apatite formation on all coatings except for 10 wt.% YSZ. Cytocompatibility was better than HA as confirmed by superior cell adhesion and proliferation.

The deposition of HA coatings has also been enhanced through the use of a supersonic plasma nozzle where HA particles are introduced into the plasma torch at 510 m/s, much higher than conventional plasma nozzle. In a traditional nozzle, the HA particles reside in the plasma for 5 ms, whereas in a supersonic nozzle they reside in the plasma for only 290 μs and hence have a reduced heat treatment (Ref 15). Roy et al. (Ref 118) investigated the effects of using a supersonic nozzle in depositing HA coating onto Ti. They found that using normal plasma nozzle increased phase decomposition, high ACP phase formation, and severe dihydroxylation of HA. ACP as previously mentioned, dissolves faster than its crystalline form and can therefore affect bioactive fixation (Ref 119, 120). While postdeposition heat treatment can recover crystallinity, due to volume changes from amorphous to crystalline phase transformation, large coating stresses can form resulting in disintegration or delamination (Ref 121). Furthermore, normal plasma nozzle increased phase decomposition with decreasing working distance due to prolonged plasma-HA interaction where the plasma impinges on the coating surface at close distances. This removes hydroxyl groups and enhances ACP phase formation. Those prepared with the supersonic nozzle had retained the crystallinity and phase purity of HA due to short plasma flame exposure and showed cell attachment and proliferation.

For reference, plasma spray parameters for both MPS/LEPS and supersonic plasma nozzle are given in Table 5.

4. Sintered Coatings

While there is a greater emphasis on recently developed plasma-sprayed coatings for biomedical applications in the current review, newly developed HA and glass ceramic sintered coatings are also discussed for comparative reasons. Although plasma spraying is the predominant method used for coating deposition in industry, sintered bead coatings have also been used for implants and were an early form of porous ingrowth surface, introduced to cementless knee replacements in the 1980s. Typically powders or beads are applied to the implant surface either by dipping the implant or by a compaction process similar to powder metallurgy. The component is then sintered at high temperature to fuse the particles together and to the substrate (Ref 122) through a diffusion process.

Recent literature in the area of sintered biocoatings focuses on enhancing previously established coatings, such as HA and 45S5 bioglass, or in developing newly sintered biocoatings. This section reviews recent efforts made toward enhancing biocoatings prepared by sintering technique, particularly HA and glass ceramic coatings.

4.1 Hydroxyapatite Coatings

One of the primary concerns in using sintering techniques to develop biocoatings is the long sintering periods

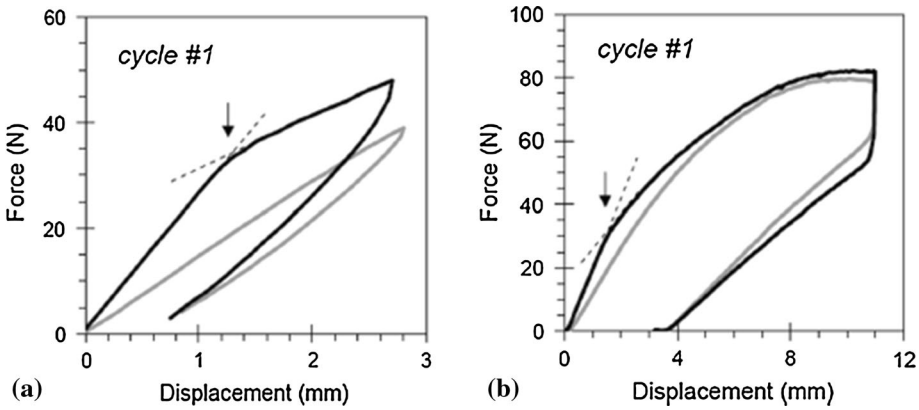

Fig. 9 Four-point bending testing: force-displacement curves for coated (black) and uncoated (gray) samples. Two successive cycles are shown for a maximum displacement of 2.8 mm (a) and 11 mm (b). Arrows indicate the slope change occurring at $\varepsilon_c = 0.9\%$ (Reprinted from Ref 116, Copyright (2014), with permission of Springer)

at elevated temperatures which cause HA to decompose into TCP and TTCP (Ref 123). As previously explained, TCP and TTCP have high dissolution rate which is a particular risk for implant fixation and stability (Ref 106). Furthermore, high localized dissolution can disturb surrounding tissue. Changing the intrinsic microstructure of HA has been shown to prevent decomposition during sintering (Ref 124-126). Song et al. (Ref 123) therefore prepared HA nano-rods and submicron prisms, compressed them into discs or cubes, and sintered them without pressure at 1150 to 1250 °C for 2 h. Ambient atmosphere with heating rate of 10 °C/min was used, and after samples were furnace cooled to minimize internal cracks, the HA nano-rods and submicron prisms showed no decomposition up to 1250 °C sintering temperature.

Another way to eradicate HA decomposition is to reduce sintering temperature or time. Ohtsu et al. (Ref 127) suggest a chemical coating process using slurry reagent and low-temperature sintering to obtain a thin HA coating on Ti substrate. CP-Ti powder was mixed with water and substrates were buried in the slurry then heated to 650 °C in air for 2 h. The substrates were then removed from the slurry, ultrasonically cleaned, and dried in air at 60 °C. A composite HA/TiO_2 coating was fabricated (microstructure shown in Fig. 10). When heated, solid-to-solid diffusion of Ca and P from the slurry into the Ti substrate was promoted resulting in the growth of the coating. Growth rate of calcium phosphate precipitate from SBF was significantly enhanced as compared to the bare control. The newly formed coating maintained cell adhesion and proliferation, and differentiation of osteoblasts into osteocytes was enhanced (Ref 128). In a later study, Ohtsu et al. (Ref 129) varied the sintering temperature from 450 to 750 °C to find ideal temperature for biocompatibility and mechanical strength. Calcium phosphate precipitated on the surface regardless of sintering temperature; however, bond strength was highest at 625 °C.

The brittle nature of HA has been another focus in terms of enhancement. Previously, efforts to enhance the brittle nature of HA were made through the addition of ZrO_2 where the biocompatibility of HA and the strength of ZrO_2 were leveraged for orthopedic applications (Ref 130, 131). Despite their combination, HA still decomposed during sintering into β-TCP and CaO. CaO is particularly undesirable because of its tendency to undergo a hydration reaction during storage or after implantation, dangerously increasing in volume by 50% (Ref 100). Furthermore, phase transformation of partially stabilized ZrO_2 from tetragonal to cubic structure occurred, diminishing the mechanical properties of the composites due to the formation of $CaZrO_3$. Pardun et al. (Ref 132, 133) reported similar findings in terms of decomposition when the composition was predominantly HA (Fig. 11); however, reasonable mechanical strength, interfacial bonding, and bioactivity were achieved for YSZ/HA coatings with ratios of 1:1 and 2:1.

Recently, Wang et al. (Ref 134) attempted to rectify these issues through the addition of TiO_2 into HA/ZrO_2 composite. 0 to 2.4 wt.% of TiO_2 was added to HA/ZrO_2 nano-powder; compacts were created; and green bodies were sintered between 900 and 1200 °C for 2 h. The addition of TiO_2 restrained HA decomposition and $CaZrO_2$ formation. As the temperature increased from 900 to 1200 °C with <0.8 wt.% TiO_2, main phases found were HA and ZrO_2. Above 1200 °C with > 0.8 wt.%, main phases were HA, ZrO_2, and a small amount of dicalcium phosphate.

The thickness and density of HA scaffolds offer superior osseointegrative function. Sultana et al. (Ref 135) therefore propose a coating-substrate cosintering process to obtain scaffold-like HA coatings on zirconia with thicknesses between 30 and 300 μm. The microporous zirconia substrate is first prepared by presintering at 900 °C for 2 h with PMMA as sacrificial pore material, then graded HA coatings are applied, and both are cosintered at 1300 °C for 2 h. Cosintering allows a strong ceramic bond between HA and zirconia due to the densification process and chemical reactions between the interface. To account for CTE differences between HA and ZrO_2, Al_2O_3 is added and compositions are varied

Table 5 Plasma spray parameters for MPS/LEPS and supersonic nozzle

Author	Powder spray distance (mm)	Flow rate Ar carrier gas (slpm)	Power (kW)	Spray voltage (V)	Spray current (A)	Flow rate primary/ secondary/ sheath gas (slpm)	Powder feed rate (g/min)
MPS/LEPS coatings							
Dey et al. (Ref 112)	HA; β-TCP75	…	<1.5	30	40	10 (Ar)/20 (Ar)/…	0.09
Dey and Mukhopadhyay (Ref 113)	HA75 to 100	…	1.5	…	40	10 (Ar)/20 (Ar)/…	0.0015
Garcia-Alonso et al. (Ref 99)	HA35 to 45	30-42	12	30	390	4.6 (Ar)/…/…	5 to 9
Garcia-Alonso et al. (Ref 99)	HA/PCL38	36	12	30	390	4.6 (Ar)/10-14 (N_2)/…	9 (HA); 0.040-0.120 (HA/PCL)
Supersonic nozzle gas							
Fielding et al. (Ref 15)	AgO_2/SrO_2 doped HA110	10	25	…	…	25 (Ar)/…/60 (Ar) + 6 (H_2)	…
Roy et al. (Ref 118)	HA110	10	25	…	…	25 (Ar)/…/60 (Ar) + 6 (H_2)	…
Roy et al. (Ref 14)	AgO_2 doped HA110	10	25	…	…	25 (Ar)/…/60 (Ar) + 6 (H_2)	…

with the substrate being 30 vol.% HA 70 vol.% YSZ. The first layer of the coating was 80 vol.% HA, 10 vol.% ZrO_2, and 10 vol.% Al_2O_3 while the outside layer was 50 vol.% HA, 40 vol.% micro HA, and 10 vol.% Al_2O_3. Microporous HA coating with 300 μm thickness was successfully deposited on zirconia (Fig. 12). Strong adhesion was confirmed through observation/testing, and bending strength was over 300 MPa.

The addition of ions has been another area of research as such trace elements are present in natural apatites of bone and are therefore assumed to enhance bioactivity by mimicking the composition of native bone more closely (Ref 30). Zn^{2+} is of particular interest as it has an important role in enzyme activity and its uptake and release are mediated by the bone reservoir in the body (Ref 136). In fact, zinc has already been shown to stimulate bone formation and mineralization (Ref 137, 138) while also having antibacterial effect (Ref 139). F^- ion has been shown to improve both biological properties (Ref 140) as well as mechanical properties (Ref 141). Zn^{2+} and F^- codoped HA was therefore investigated, where samples were sintered at 1100 °C for 1 h (Ref 142). Co-doping improved the mechanical properties of pure HA. The additions of Zn^{2+} and F^- enhanced the bioactivity of HA. Apart from the addition of trace elements in ionic form, 45S5 bioglass has also been combined with HA in an effort to improve bioactivity (Ref 143). According to one study, 45S5 has shown to have higher bone forming ability than HA due to surface reactions (Ref 144). The composites sintered at 1200 °C for 4 h had increased decomposition of HA to TCP which then degraded to calcium and phosphate salts and reprecipitated as an apatite layer (Ref 145). At increased 45S5 content, $Na_3Ca_6(PO_4)_5$ crystalline phase formed in a mixture of sodium silicate and calcium phosphate matrix which induced increased bioactivity because of their higher solubility that form HCA faster, an indicator for early bone growth rate and new bone formation (Ref 98).

4.2 Glass Ceramic Coatings

Sintering of bioactive glass is often scrutinized as the high sintering temperatures of 1000 to 1300 °C cause coating decomposition and form new undesired phases (Ref 146, 147). These high-temperature treatments can cause crystallization into glass ceramic prior to complete densification and have shown adverse effects on bioactivity (Ref 148, 149). Both composition and amorphous nature of bioactive glass control their bioactivity. Various studies have recently focused on modifying traditional 45S5 bioglass to achieve lower sintering temperatures. Bellucci et al. (Ref 150) introduce a novel bioactive glass called BioK (46.1 mol.% SiO_2, 26.9 mol.% CaO, 24.4 mol.% K_2O (which substituted Na_2O in 45S5), and 2.6 mol.% P_2O_5) with reduced tendency to crystallize as compared to 45S5 bioglass (Ref 151), belonging to the same family. Through the substitution of Na_2O in 45S5 by K_2O, the new bioactive glass has low tendency to crystallize. 50 wt.% BioK/HA and 50 wt.% 45S5/HA green bodies were prepared. BioK/HA consolidated at a low

sintering temperature of 750 °C (5 °C/min heating rate) for 3 h before crystallization phenomena could occur as compared to 1150 °C for HA/45S5. The new composite had positive effect on bioactivity evaluated by SBF immersion, superior to 45S5. The same authors investigated yet another 45S5 bioglass modified glass-HA composite with lower sintering temperature (800 °C) (Ref 152). BG_Ca is composed of 47.3 mol.% SiO_2, 45.6 mol.% CaO, 4.6 mol.% Na_2O, and 2.6 mol.% P_2O_5, which has a reduced tendency to crystallize as compared to traditional 45S5 Bioglass. Up to 80 wt.% HA-BG_Ca composites could be sintered at 800 °C as compared to 1150 °C for HA-45S5. The lower temperature preserves the amorphous nature of the glass which improved bioactivity. Furthermore reactions between glass and HA as well as HA decomposition are prevented at lower sintering temperatures. Improved vitro bioactivity and biocompatibility were obtained for 20 and 40 wt.% HA-BG_Ca composites. HA-BG_Ca showed earlier response of cell proliferation as compared to HA-45S5. Similar work was undertaken by Xie et al. (Ref 153) where 45S5 and $Na_2Ca_2Si_3O_9$-based bioglasses were modified to lower sintering temperature through the addition of B_2O_3 to ≤900 °C, while preserving bioactivity and improving mechanical properties. Figure 13(a) shows that all $Na_2Ca_2Si_3O_9$-based bioglasses with up to ~4 wt.% B_2O_3 had improved mechanical properties while maintaining HA growth as observed by XRD (Fig. 13b).

Kirsten et al. (Ref 154) similarly modified the composition of 45S5 bioglass to form an ideal bioactive and thermally compatible coating for zirconia dental implants through tailored substitution of alkaline earth metals and alkaline metals (Fig. 14). The demand for ceramic dental implants is increasing for esthetic reasons as compared to metal implants (Ref 155) and because patients prefer metal-free implants (Ref 156). 45S5 in its current composition is not suitable for thermal coating process on zirconia because of its high crystallization tendency and its high CTE (15×10^{-6}/K) (Ref 157) as compared to zirconia (10.8 to 12.5 $\times 10^{-6}$/K) (Ref 158, 159). The goal is to partially replace CaO by MgO and Na_2O by K_2O to obtain a bioactive coating with similar CTE as zirconia. The prepared glass coatings were deposited using a spray nozzle, then were sintered at 800 °C for 100 min to obtain a dense primary layer, then were sprayed again, and sintered at 760 °C for 10 min to obtain a microstructured second layer. A coating thickness of 20 to 50 μm was achieved. CTE was well adjusted to ~0.09×10^{-6}/K less than zirconia CTE. The primary layer was densely sintered without any crystallization, and no crack or delamination was found. Good bonding between the first and second layers was also found. SBF tests revealed comparable Ca/P-rich layers with similar thickness and morphology as gold standard 45S5 bioglass. In terms of cytotoxicity, the novel coating was cytocompatible having no harm to cells as determined by proliferation test of seeded mouse fibroblasts.

Lee et al. (Ref 160) have adjusted 45S5 bioactive glass to form BGS-7 and compared it to HA coatings. The chemical composition of BGS-7 is CaO 41.8, SiO_2 35.8, P_2O_5 13.9, B_2O_3 0.5, CaF_2 2.0, and MgO 6.0 (wt.%). S-pins, widely used in orthopedic surgery for fracture treatment or reconstructive surgery after osteotomy, were dip-coated using prepared slurries of BGS-7 and HA then sintered at ~875 and 500 °C for 1 h, respectively. Coating thicknesses were ~30 μm and ~550 nm for BGS-7 and HA,

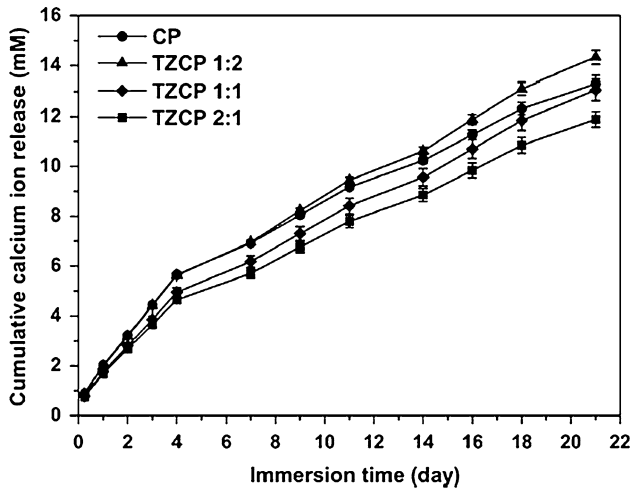

Fig. 11 Dissolution behaviour of pure HA (CP) and YSZ-HA at varying YSZ:HA ratios (Reprinted from Ref 132, Copyright (2015), with permission from Elsevier)

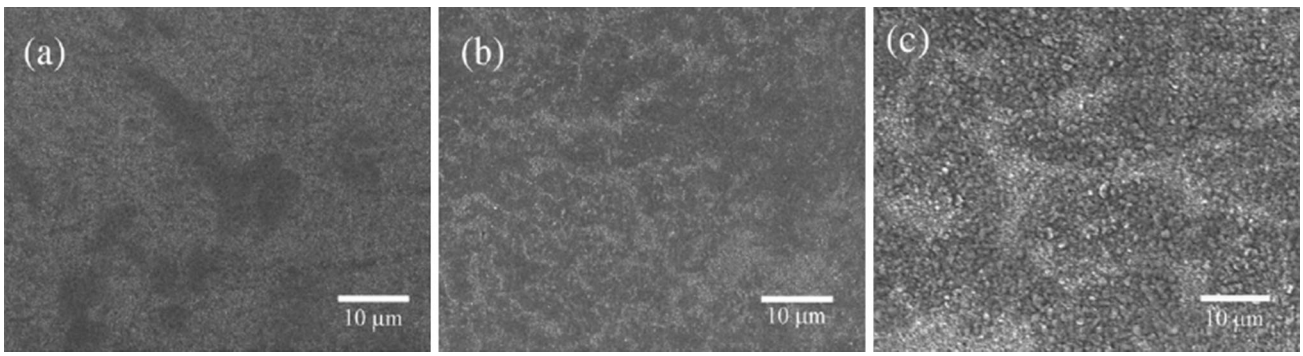

Fig. 10 SEM micrograph of Ti surface treated by calcium phosphate slurry at (a) 500 °C, (b) 625 °C, and (c) 750 °C (Reprinted from Ref 129, Copyright (2014), with permission from Elsevier)

respectively. At all test points, BGS-7 bone-implant contact ratio following implantation in a rabbit model was higher than HA. The ultimate tensile strength of BGS-7 was higher than HA at all time points as well. Following this study, the same authors proceeded to look at different bioactive ceramic compositions (mol.%) (Fig. 15) and found that CPP and BGS-7 coated on cancellous screws inserted into tibia and femur of canine were most successful at directly bonding to cancellous bone than uncoated screws (Ref 161). Coating slurries were used and were sintered at 750 to 850 °C in a vacuum atmosphere.

Apart from 45S5 bioglass system, calcium-silicate glass ceramic systems have also shown promise as biocoatings but are limited due to their high dissolution rate (Ref 82). To eradicate the high dissolution of $CaSiO_3$ ceramic coatings, $CaSiO_3$/polymer composites were fabricated (Ref 162). $CaSiO_3$ can be fabricated by sintering compacted powders without pressure, in air at 1100 °C for 3 h at a heating rate of 2 °C/min, then cooling the samples at room temperature. Following preparation of $CaSiO_3$, the pucks were dipped in PLGA (polylactic-co-glycolic acid) polymer solution and dried at 60 °C for 1 day. PLGA is widely used for biomedical applications (Ref 163, 164). Through the addition of the modified polymer layer, the degradation of the calcium-silicate was reduced while maintaining the apatite forming ability of the ceramic.

Baino et al. (Ref 165) aimed to develop glass ceramic coating by sintering technique with adequate adhesion using new airbrush spray method. Prepared SCNA ($57SiO_2$-$34CaO$-$6Na_2O$-$3Al_2O_3$, wt.%) slurries with different compositions (Fig. 16) were deposited onto alumina substrates using airbrush spray gun at 3.5×10^5 Pa for 2 s and then the green layers were dried for 1 h. The coatings were then sintered at 1000 °C for 3 h at a heating rate of 5 °C/min and cooling rate of 10 °C/min. The adhesion was approximately 30 MPa which is more than double the ASTM threshold for bioceramic coatings. The authors also propose a model for the newly developed airbrush spraying method in combination with sintering. The number of spraying cycles (N) required to achieve coating thickness (t) can be determined by $t = CN$, where C is the model constant determined by the authors (Fig. 17).

Development of new glass ceramic coatings has also been driven by antimicrobial property. Calcium-strontium-zinc-silicate glasses coupled with ionic substitution have been shown to release controlled amounts of Zn^{2+} and Sr^{2+} ions when placed in physiological conditions. The level of the ion release correlates well with the levels typically associated with clinical benefits (Ref 166, 167). Furthermore, antibacterial properties, cell viability, and osseointegration are enhanced by these elements (Ref 166, 168). The disadvantage of these glasses is their lack in providing strength for load-bearing applications. Looney et al. (Ref 169) particularly focused on enhancing the sintering cycle to maximize the mechanical strength of three glass ceramics while also investigating antibacterial property (Fig. 18). Optimum sintering temperatures of 1000, 970, and 900 °C for BT110, BT111, and BT112, respectively, were used (Fig. 18). They were heated at 5 °C/min in helium atmosphere and held at optimum sintering temperature for 3 h and then cooled at 10 °C/min. Biaxial flexural strength ranged from 70 to 149 MPa exceeding those clinically established by HA and pure β-TCP. BT112 in particular showed inhibitory effect against three of the most common bacteria found after implantation.

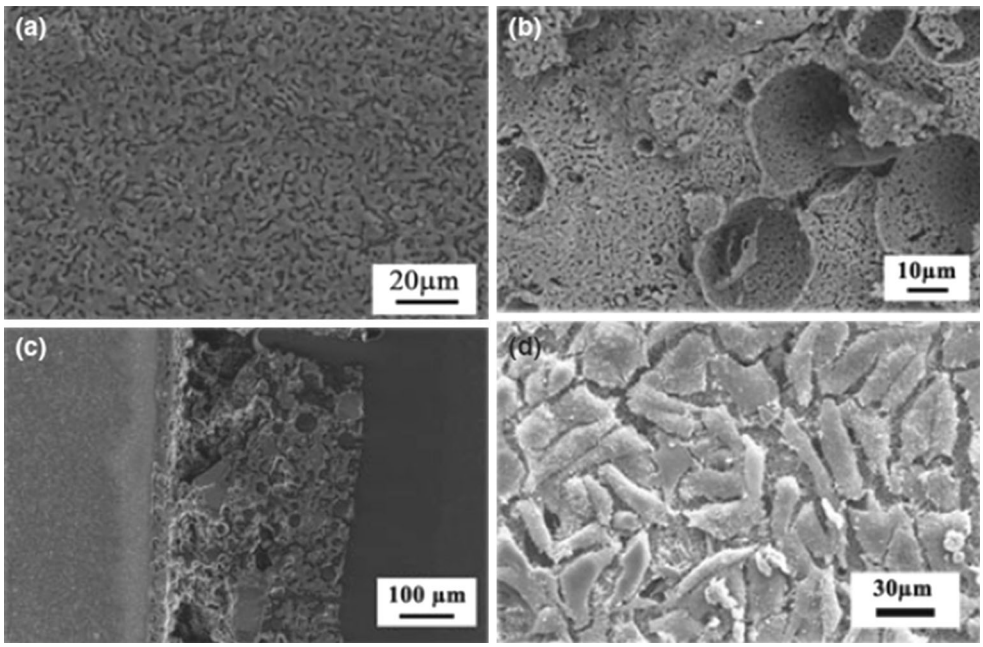

Fig. 12 SEM micrograph of (a) surface morphology HA coating, (b) large pores from PMMA particles, (c) HA coating cross section, and (d) osteoblast growth after 3 days (Ref 135. Copyright © 2012 by John Wiley Sons, Inc. Reprinted by permission of John Wiley & Sons, Inc.)

Other antimicrobial glass coatings have also been studied, particularly those belonging to B_2O_3-SiO_2-Na_2O-ZnO and SiO_2-Na_2O-Al_2O_3-CaO-B_2O_3 systems (Fig. 19) (Ref 170). CTE mismatch was adjusted by changing glass compositions as well as sintering atmosphere (air or Ar). The coatings were deposited on Ti-6Al-4V (air and Ar), tantalum, niobium (Ar to avoid oxidation), and 316L SS substrates (air). Green coatings were sintered in air and Ar at 725 °C for ZnO_{15}, 630 °C for ZnO_{35}, and 750 °C for G3 heated at 10 °C/min. Antimicrobial properties against *E. coli* for ZnO_{15} coating were good on all substrates, but better for those sintered in Ar gas as no bubbles formed. Similar results were found for ZnO35 coatings expect on Ti-6Al-4V substrates due to poor adherence. For G3 coatings, good results were only found on 316L SS.

4.3 Other Coatings

While most sintered biocoatings focus on HA and glass ceramics, Mutlu (Ref 171) developed a method to simultaneously sinter Ti foams for bone replacement applications while coating the foam with a biocompatible TiN layer. TiN is of interest as it has excellent corrosion and wear resistance, is biocompatible, has good adhesion, and can be used as a hard coating on load-bearing implants (Ref 172-176). The coating was fabricated by sintering the foam in N_2 atmosphere at 1200 °C. Various techniques such as PVD, ion beam deposition, plasma spraying have been used to produce TiN films; however, through this combined sinter-coating process, both cost and time are reduced. An increase in mechanical properties of coated foams was observed as compared to the control.

4.4 Sintering Temperatures

Hung et al. (Ref 177) specifically studied the sintered microstructure of calcium phosphate powders with Ca/P ratio of 1.50 as opposed to hydroxyapatite ($Ca_{10}(PO_4)_6(OH)_2$) with 1.67 ratio. When pellet samples were sintered between 600 and 1200 °C for 4 h, HA remained the major phase with some rhenanite ($NaCaPO_4$) and minor β-TCP (β-$Ca_3(PO_4)_2$). At sintering temperatures of 1300 to 1400 °C for 4 h, the HA partially transformed to α-TCP (α-$Ca_3(PO_4)_2$) and TTCP ($Ca_4(PO_4)_2O$). Evidently, higher temperatures cause unwanted decomposition.

4.5 Modified Sintering Technologies

New sintering technologies such as spark plasma sintering (SPS), have been developed to improve the sintering technique, particularly focusing on reducing sintering time and elevated temperatures. Conventional sintering is particularly disadvantageous because of the long sintering period at elevated temperatures which has been shown to cause HA to decompose into TCP and TTCP (Ref 123). Conventional sintering supplies heat to the sample externally, whereas SPS uses a DC current to generate heat

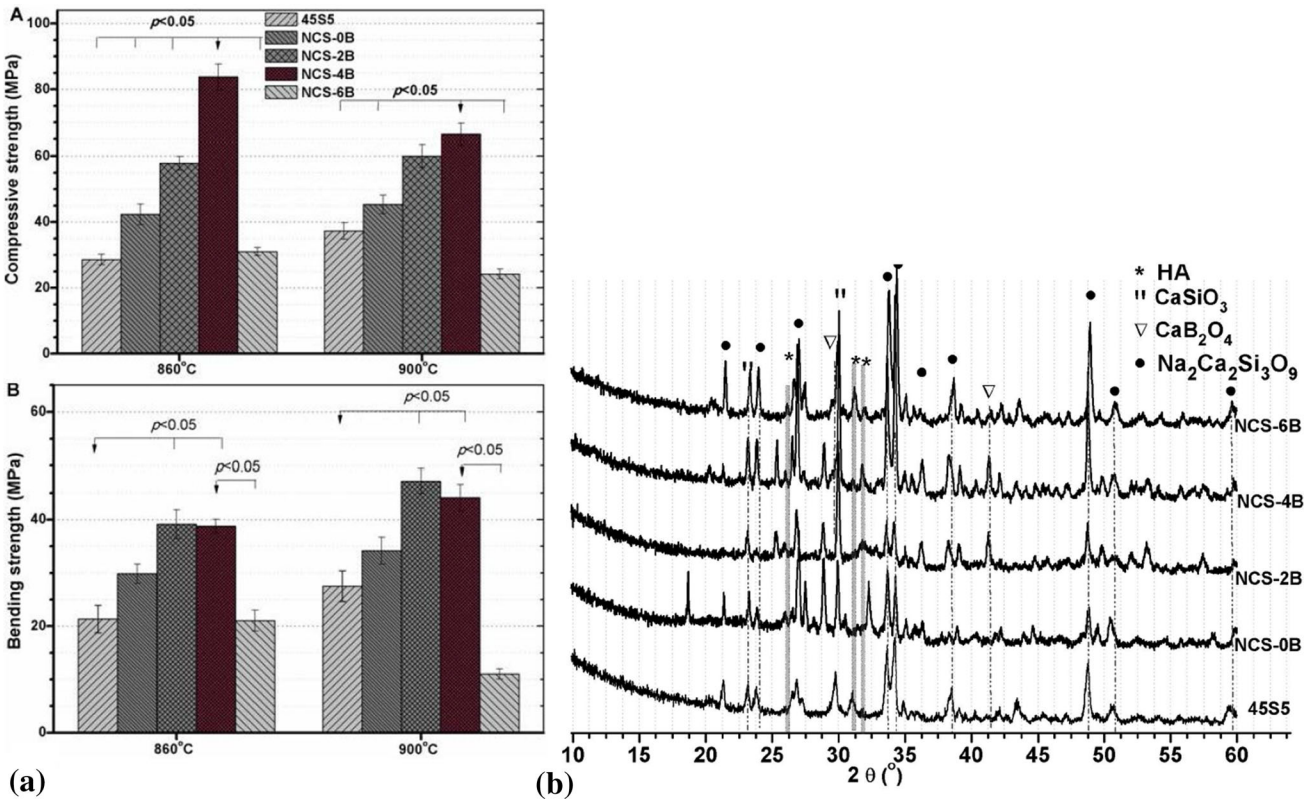

Fig. 13 (a) Mechanical properties and (b) post-SBF immersion XRD of 45S5 and $Na_2Ca_2Si_3O_9$-based bioglasses (Ref 153, Fig. 5 and 7)

internally and significantly reduces sintering time from hours to minutes while allowing nano-structures to be retained. SPS has been used to deposit α-TCP and β-TCP powders (Ref 178), both commonly used in clinical applications such as dentistry, maxillofacial surgery, and orthopedics. For example, Mondal et al. (Ref 178) fabricated homogenous 30, 50, and 70 vol.% CP-Ti/TCP composites. Using SPS, the samples were heated to a sintering temperature of 1200 °C at a heating rate of 192 °C/min and a constant uniaxial pressure of 50 MPa was applied to the powder. After sintering the sample was cooled below 100 °C within 12 min. The mechanical properties of the composites were similar to human cortical bone and biocompatibility was enhanced with increasing TCP vol.% as indicated by increased cell adhesion, proliferation, and in vivo bone formation. In another study, SPS was used in fabricating graphene-reinforced HA samples. Graphene was added to serve as a second-phase reinforcement for improved mechanical properties. It is also a favorable candidate because of its unique structural features, its ability to be functionalized and low risk of impurity-induced toxicity (Ref 179). The sintering was carried out in vacuum at 950 °C, 30 MPa with a 3-min processing time. Both mechanical properties and in vitro bioactivity were improved by the addition of graphene. The improvement in mechanical properties is shown below (Fig. 20), in addition to an illustration explaining how the addition of graphene impeded crack propagation (Fig. 21).

The technology has also been used in preparing zirconia/titanium composites (Ref 180). Zirconia and titanium are of interest in dental and orthopedic applications due to the integrative nature with host tissue (Ref 181-184). However, the two are yet to be combined due to limitations set by conventional sintering where both phases would react with one another and the atmospheric gas,

	45S5		PC-XG3	
Oxide	Targeted Composition (wt%)	Actual Composition (wt%)	Targeted Composition (wt%)	Actual Composition (wt%)
SiO_2	45	45.53	45	44.84
CaO	24.5	24.88	22.5	21.81
MgO	—	0.06	17	17.72
Na_2O	24.5	23.18	—	0
K_2O	—	0	9.5	9.41
P_2O_5	6	6.29	6	6.15
Impurities	—	0.06	—	0.07

Fig. 14 Glass ceramics studied by Kirsten et al. (Ref 154, copyright © 2015 by SAGE Publications, Inc. Reprinted by Permission of SAGE Publications, Inc.)

Parameter	Group A	Group B	Group C	Group D
Abbreviation	CPP	W3G	CSG	BGS-7
Chemical composition	$Ca_2P_2O_7$	CaO 55.5%, SiO_2 39.8%, P_2O_5 4.7%	CaO 45.8%, SiO_2 45.8%, B_2O_3 8.4%	MgO 5.97%, CaO 41.97%, SiO_2 35.82%, P_2O_5 13.93%, CaF_2 1.99, B_2O_3 0.5%

Fig. 15 Chemical composition and abbreviation of each group (Reprinted from Ref 161, Copyright (2011), with permission of Springer)

Slurry	Composition (wt%)			
	SCNA powder	Water	PVA	Glycerine
A	50	50	–	–
B	30	70	–	–
C	30	64	–	6
D	30	64	6	–
E	50	40	3	7

Fig. 16 SCNA slurries deposited by airbrush spray then sintered (Reprinted from Ref 165, Copyright (2015), with permission from Elsevier)

Slurry	C (μm)	R^2
Slurry B	3.686	0.93
Slurry D	27.160	0.92
Slurry E	28.023	0.89

Fig. 17 Airbrush spraying model parameter (C) for desired coating thickness (Reprinted from Ref 165, Copyright (2015), with permission from Elsevier)

Glass	SiO_2	ZnO	CaO	SrO	Na_2O
BT110	0.4	0.2	0.1	0.2	0.1
BT111	0.4	0.1	0.1	0.2	0.2
BT112	0.4	0	0.1	0.2	0.3

Fig. 18 Glass ceramics (mol.%) studied by Looney et al. (Ref 169, copyright © 2011 by SAGE Publications, Inc. Reprinted by Permission of SAGE Publications, Inc.)

Glass	SiO_2	B_2O_3	Na_2O	CaO	Al_2O_3	K_2O	ZnO
ZnO15	29.4	45.0	8.2	–	4.6	–	12.8
ZnO35	23.1	35.3	6.4	–	3.6	–	31.6
G3	43.0	7.8	19.4	22.0	7.4	0.4	–

Fig. 19 Glass ceramics (mol.%) studied by Tejeda et al. (Reproduced with permission from Ref 170.)

forming unwanted side compounds which weaken the structure (Ref 185, 186). With the use of SPS fast material consolidation reduces reactivity and maintains grain size similar to starting powders. Therefore (0, 25, 50, 70, 100 wt.%) 3 Y-TZP/Ti composites were fabricated using SPS at 1350 °C, 80 MPa for 10 min at a heating rate of 100 °C/min to form dense specimens (Ref 180). It was found that these composites had highest osteoblast proliferation and differentiation at longer culture times as compared to titanium and zirconium prepared separately.

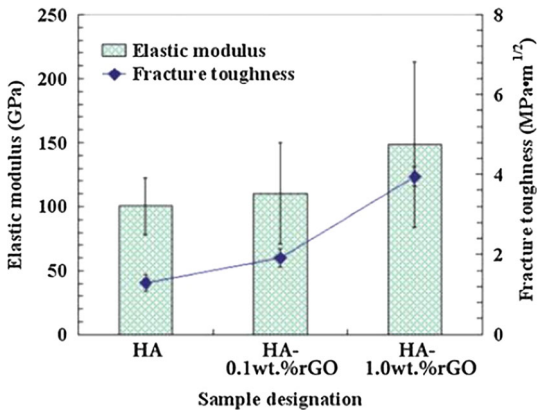

Fig. 20 Mechanical properties of HA and HA-reduced graphite oxide (rGO) (Reproduced from Ref 179, with permission of The Royal Society of Chemistry)

5. Conclusions

Biocoatings have been in use for decades now, yet the literature surrounding the topic continues to grow as new materials and processes to enhance existing biocoatings are made available. The current review focuses on new or enhanced biocoatings, particularly HA and glass ceramics, prepared by plasma spray and sintering techniques within the past 5 years.

Recently developed plasma spray and sintered coatings have focused on incorporating elements found in natural bone matrix with the objective of replicating the role of those elements in the skeletal system. Some of those elements include Si (Ref 13), Zinc (Ref 82, 88, 142), and Mg (Ref 91), which among other elements found in bone, were shown to improve HA and glass coatings. Another

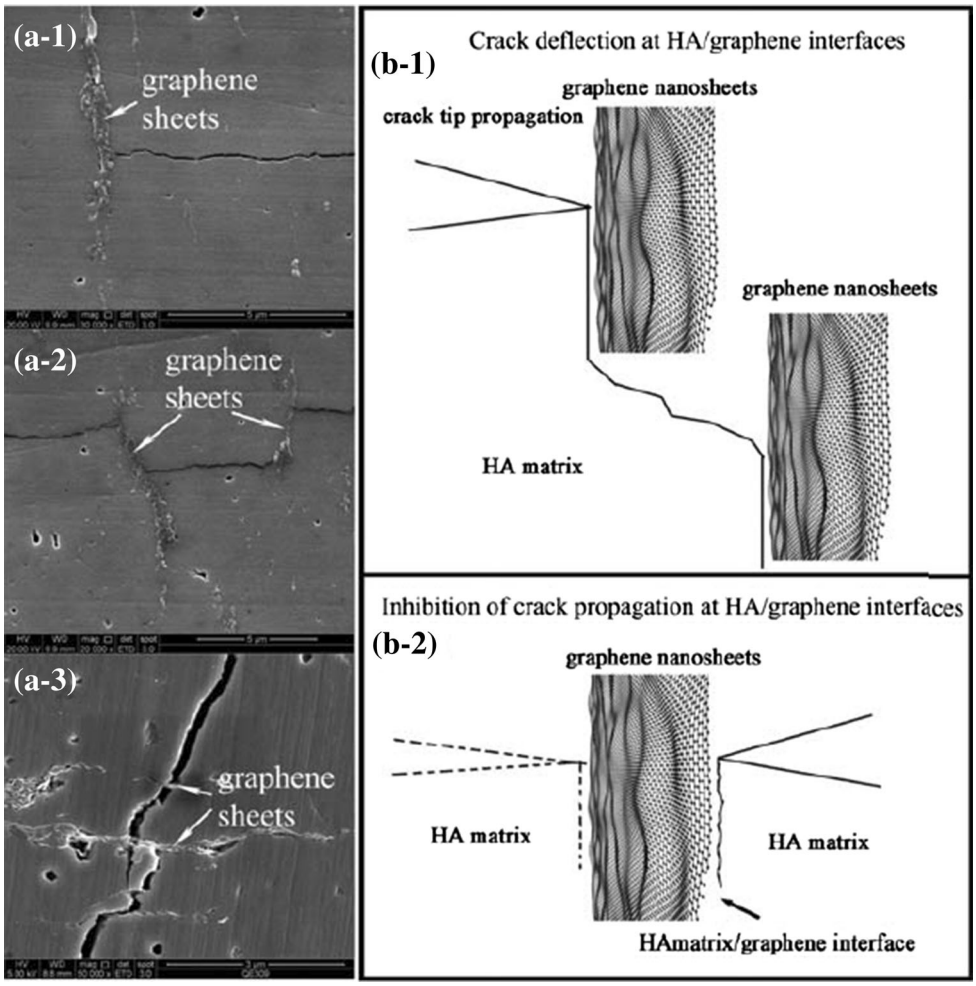

Fig. 21 Crack impedance by graphene nano-sheets in HA-rGO composites. (a-1, b-1) Termination of crack growth by graphene nano-sheets at crack tip, (a-2, b-2) Deflection of crack by graphene nano-sheets, and (a-3) Bridging of the crack by graphene nano-sheets (Reproduced from Ref 179, with permission of The Royal Society of Chemistry)

main area of research was on bacterial growth resistance, an important aspect in reducing the risk of prosthetic joint infection. In addition to investigating the effects of varying amounts of Ag, the addition of other dopants was shown to also improve bacterial resistance, among other properties. These dopants include CeO_2 (Ref 63), Zn, and Sr (Ref 169). For both plasma-sprayed and sintered biocoatings, the efforts to reduce CTE mismatch between coatings and substrates were evident among the literature. This was generally achieved by the addition or replacement of compounds and was more prominent in glass ceramics where Zn, Ti (Ref 88), and Mg (Ref 91, 154) successfully reduced CTE mismatch. Incorporation of a buffer layer was also effective (Ref 70, 135). Various methods to reduce the sintering temperature of glass ceramics have been found over the past 5 years. Several studies have modified 45S5 to lower sintering temperature through compound substitutions such as K_2O (Ref 150) and B_2O_3 (Ref 153). These new coatings show great promise, delivering better performance than 45S5 itself. Though HA and 45S5 Bioglass were once regarded as the golden standard in biocoatings, with time these coatings have evolved and will continue to do so as their advantages are leveraged while the disadvantages are alleviated through the addition of dopants.

Apart from the new coating materials developed within the past 5 years, processing technologies in plasma spraying and sintering have advanced. Both methods are often scrutinized due to high-temperature exposure, and for sintering over a long period of time. While APS is still traditionally used in the mainstream coating development, MPS and LEPS with low plasma power have proven to be useful in reducing the harmful effects of high temperatures and in spraying polymers. Supersonic plasma nozzles can also be used to reduce the effects of high temperatures by reducing the residence time of the powder particle in the plasma. For sintering, SPS has been equally effective at alleviating high-temperature exposure by reducing the sintering time to minutes. These technologies can be useful in avoiding undesired degradation of HA and glass

ceramic coatings. While they are not the traditional methods used in practice, increased experimentation with these technologies is expected.

References

1. A. Kobayashi, W. Donnelly, G. Scott, and M. Freeman, Early Radiological Observations May Predict the Long-Term Survival of Femoral Hip Prostheses, *J. Bone Joint Surg. Br.*, 1997, **79B**, p 583-589
2. L. Hench, Bioceramics: From Concept to Clinic, *J. Am. Ceram. Soc.*, 1991, **74**, p 1487-1510
3. S. Goodman, Z. Yao, M. Keeney, and F. Yang, The Future of Biologic Coatings for Orthopaedic Implants, *Biomaterials*, 2013, **34**, p 3174-3183
4. S.Y.F. Hulbert, R. Mathews, J. Klawitter, C. Talbert, and F. Stelling, Potential of Ceramic Materials as Permanently Implantable Skeletal Prostheses, *J. Biomed. Mater. Res.*, 1970, **4**, p 16-24
5. S. Santavirta, J. Xu, J. Hietanen, A. Ceponis, T. Sorsa, R. Kontio, and Y. Konttinen, Activation of Periprosthetic Connective Tissue in Aseptic Loosening of Total Hip Replacements, *Clin. Orthop. Relat. Res.*, 1998, **352**, p 16-24
6. A. Oliveira, J. Mano, and R. Reis, Nature-Inspired Calcium Phosphate Coatings: Present Status and Novel Advances in the Science of Mimicry, *Curr. Opin. Solid State Mater. Sci.*, 2003, **7**, p 309-318
7. M. Jasty, C. Bragdon, D. Burke, D. O'Connor, J. Lowenstein, and W. Harris, In Vivo Skeletal Responses to Porous-Surfaced Implants Subjected to Small Induced Motions, *J. Bone Joint Surg. Am.*, 1997, **79**, p 707-714
8. M. Tanahashi and T. Matsuda, Surface Functional Group Dependence on Apatite Formation on Self-Assembled Monolayers in a Simulated Body Fluid, *J. Biomed. Mater. Res.*, 1997, **34**, p 305-315
9. T. Kokubo, F. Miyaji, H. Kim, and T. Nakamura, Spontaneous Formation of Bonelike Apatite Layer on Chemically Treated Titanium Materials, *J. Am. Ceram. Soc.*, 1996, **79**, p 1127-1129
10. R. Viitala, M. Jokinen, T. Peltola, K. Gunnelius, and J. Rosenholm, Surface Properties of In Vitro Bioactive and Non-Bioactive Sol-Gel Derived Materials, *Biomaterials*, 2002, **23**, p 3073-3086
11. S. Mistry, D. Kundu, S. Datta, D. Basu, and C. Soundrapandian, Indigenous Hydroxyapatite Coated and Bioactive Glass Coated Titanium Dental Implant System—Fabrication and Application in Humans, *J. Indian Soc. Periodontol.*, 2011, **15**, p 215-220
12. G. Rizzi, A. Scrivani, M. Fini, and R. Giardino, Biomedical Coatings to Improve the Tissue-Biomaterial Interface, *Int. J. Artif. Organs*, 2004, **27**, p 649-657
13. E. Karamian, M. Motamedi, A. Khandan, P. Soltani, and S. Maghsoudi, An In Vitro Evaluation of Novel NHA/Zircon Plasma Coating on 316L Stainless Steel Dental Implant, *Prog. Nat. Sci. Mater. Int.*, 2014, **24**, p 150-156
14. M. Roy, G. Fielding, H. Beyenal, A. Bandyopadhyay, and S. Bose, Mechanical, In Vitro Antimicrobial, and Biological Properties of Plasma-Sprayed Silver-Doped Hydroxyapatite Coating, *Appl. Mater Interfaces*, 2012, **4**, p 1341-1349
15. G. Fielding, M. Roy, A. Bandyopadhyay, and S. Bose, Antibacterial and Biological Characteristics of Plasma Sprayed Silver and Strontium Doped Hydroxyapatite Coatings, *Acta Biomater.*, 2012, **8**, p 3144-3152
16. C. Wu, J. Chang, S. Ni, and J. Wang, In Vitro Bioactivity of Akermanite Ceramics, *J. Biomed. Mater. Res. A*, 2006, **76A**, p 73-80
17. A. Posner, The Mineral of Bone, *Clin. Orthop. Relat. Res.*, 1985, **200**, p 87-99
18. D.D.N. Vandiver, C. Patel, S. Botelho, J. Best, M. Santos, W. Lopes, W. Bonfield, and C. Ortiz, Silicon Addition to Hydroxyapatite Increases Nanoscale Electrostatic, van der Waals, and Adhesive Interactions, *J. Biomed. Mater. Res. A*, 2006, **78A**, p 352-363
19. C. Bothelo, M. Lopes, I. Gibson, S. Best, and J. Santos, Structural Analysis of Si-Substituted Hydroxyapatite: Zeta Potential and X-ray Photoelectron Spectroscopy, *J. Mater. Sci. Mater. Med.*, 2002, **13**, p 1123-1127
20. N. Hijon, V. Cabanas, J. Pena, and M. Vallet-Regi, Dip Coated Silicon-Substituted Hydroxyapatite Films, *Acta Biomater.*, 2006, **2**, p 567-574
21. I. Gibson, K. Hing, S. Best, and W. Bonfield, Enhanced In Vitro Cell Activity and Surface Apatite Layer Formation on Novel Silicon Substituted Hydroxyapatites, *12th International Symposium on Ceramics in Medicine*, Nara, Japan, 1999
22. A. Porter, N. Patel, J. Skepper, S. Best, and W. Bonfield, Comparison of In Vivo Dissolution in Hydroxyapatite and Silicon-Substituted Hydroxyapatite Bioceramics, *Biomater*, 2003, **24**, p 4609-4620
23. M. Lopez-Alvarez, E. Solla, P. Gonzalez, J. Serra, B. León, A. Marques, and R. Reis, Silicon-Hydroxyapatite Bioactive Coatings (Si-HA) from Diatomaceous Earth and Silica. Study of Adhesion and Proliferation of Osteoblast-Like Cells, *J. Mater. Sci. Mater. Med.*, 2009, **254**, p 1131-1136
24. E. Solla, P. Gonzalez, J. Serra, S. Chiussi, B. Leon, and J. Garcia Lopez, Pulsed Laser Deposition of Silicon Substituted Hydroxyapatite Coatings from Synthetical and Biological Sources, *Appl. Surf. Sci.*, 2007, **254**, p 1189-1193
25. S. Omelon, M. Ariganello, E. Bonucci, M. Grynpas, and A. Nanci, A Review of Phosphate Mineral Nucleation in Biology and Geobiology, *Calcif. Tissue Int.*, 2013, **93**, p 382-396
26. J. Xu, D. Joguet, J. Cizek, K. Khor, H. Liao, C. Coddet, and W. Chen, Synthesis and Characterization on Atomphospheric Plasma Sprayed Amorphous Silica Doped Hydroxyapatite Coatings, *Surf. Coat. Technol.*, 2012, **206**, p 4659-4665
27. S. Dahl, P. Allain, P. Marie, Y. Mauras, G. Boivin, P. Ammann, Y. Tsouderos, P. Delmas, and C. Christiansen, Incorporation and Distribution of Strontium in Bone, *Bone*, 2001, **28**, p 446-453
28. S. Tsuboi, H. Nakagaki, K. Ishiguro, K. Kondo, M. Mukai, C. Robinson, and J. Weatherell, Magnesium Distribution in Human Bone, *Calcif. Tissue Int.*, 1994, **54**, p 34-37
29. E. Pellegrino and R. Biltz, Bone Carbonate and the Ca to P Molar Ratio, *Nature*, 1968, **219**, p 1261-1262
30. J. Beattie and A. Avenell, Trace Element Nutrition and Bone Metabolism, *Nutr. Res. Rev.*, 1992, **5**, p 167-188
31. S. Cazalbou, C. Combes, D. Eichert, and C. Rey, Adaptative Physico-Chemistry of Bio-Related Calcium Phosphates, *J. Mater. Chem.*, 2004, **14**, p 2148-2153
32. L. Muller and F. Muller, Preparation of SBF with Different Content and Its Influence on the Composition of Biomimetic Apatites, *Acta Biomater.*, 2006, **2**, p 181-189
33. J. Reginster, Strontium Ranelate in Osteoporosis, *Curr. Pharm. Des.*, 2002, **8**, p 1907
34. S. Verberckmoes, M. De Broe, and P. D'Haese, Dose-dependant Effects of Strontium on Osteoblast Function and Mineralization, *Kidney Int.*, 2003, **2003**, p 534-543
35. E. Bonnelye, A. Chabadel, F. Saltel, and P. Jurdic, Dual Effect of Strontium Ranelate: Stimulation of Osteoblast Differentiation and Inhibition of Osteoclast Formation and Resorption In Vitro, *Bone*, 2008, **42**, p 129-138
36. L. Li, X. Ly, Y. Meng, and C. Weyant, Comparison Study of Biomimetic Strontium-Doped Calcium Phosphate Coatings by Electrochemical Deposition and Air Plasma Spray: Morphology, Composition and Bioactive Performance, *J. Mater. Sci. Mater. Med.*, 2012, **23**, p 2359-2368
37. R. Palanivelu and A. Kumar, Scratch and Wear Behaviour of Plasma Sprayed Nano Ceramics Bilayer Al_2O_3-13 wt%TiO_2/Hydroxyapatite Coated on Medical Grade Titanium substrates in SBF Environment, *Appl. Surf. Sci.*, 2014, **315**, p 372-379
38. E. Jordan, M. Gell, Y. Sohn, D. Goberman, L. Shaw, S. Jiang, M. Wang, T. Xiao, Y. Wang, and P. Strutt, Fabrication and Evaluation of Plasma Sprayed Nanostructured alumina-Titania Coatings with Superior Properties, *Mater. Sci. Eng. A*, 2001, **301**, p 80-89
39. G. Zhao, L. Xia, G. Wen, L. Song, X. Wang, and K. Wu, Microstructure and Properties of Plasma-Sprayed Bio-Coatings on a Low-Modulus Titanium Alloy from Milled HA/Ti Powders, *Surf. Coat. Technol.*, 2012, **206**, p 4711-4719
40. G. Singh, H. Singh, and B. Sidhu, In Vitro Corrosion Investigations of Plasma-Sprayed Hydroxyapatite and Hydroxyapatite-

Calcium Phosphate Coatings on 316L SS, *Bull. Mater. Sci.*, 2014, **37**, p 1519-1528
41. H. Darwiche, W. Barsoum, A. Klika, V. Krebs, and R. Molloy, Retrospective Analysis of Infection Rate After Early Reoperation in Total Hip Arthroplasty, *Clin. Orthop. Relat. Res.*, 2010, **468**, p 2392-2396
42. A. Kazachenko, A. Legler, O. Per'yanova, and Y. Vstavskaya, Synthesis and Antimicrobial Activity of Silver Complexes with Histidine and Tryptophan, *Pharm. Chem.*, 2000, **34**, p 257-258
43. J. Coulombe, H. Faure, B. Robin, and M. Ruat, In Vitro Effects of Strontium Ranelate on the Extracellular Calcium-Sensing Receptor, *Biochem. Biophys. Res. Commun.*, 2004, **323**, p 1184-1190
44. E. Brown, Is the Calcium Receptor a Molecular Target for the Actions of Strontium on Bone?, *Osteop. Int.*, 2003, **14**, p 25-34
45. S. Tat, J. Pelletier, F. Mineau, J. Caron, and J. Martel-Pelletier, Strontium Ranelate Inhibits Key Factors Affecting Bone Remodeling in Human Osteoarthritic Subchondral Bone Osteoblasts, *Bone*, 2011, **49**, p 559-567
46. K. Brammer, C. Frandsen, and S. Jin, TiO_2 Nanotubes for Bone Regeneration, *Trends Biotechnol.*, 2012, **30**, p 315-322
47. X. Li, L. Wang, Y. Fan, Q. Feng, F. Cui, and F. Watari, Nanostructured Scaffolds for Bone Tissue Engineering, *J. Biomed. Mater. Res. A*, 2013, **101**, p 2424-2435
48. B. Sjostrom, A. Brydone, R.D. Meek, and M. Dalby, Titanium Nanofeaturing for Enhanced Bioactivity of Implanted Orthopedic and Dental Devices, *Nanomedicine*, 2013, **8**, p 89-102
49. E. Christenson, Nanobiomaterial Applications in Orthopedics, *J. Orthop. Res.*, 2007, **25**, p 11-22
50. L. McNamara, R. McMurray, M. Biggs, F. Kantawong, R. Oreffo, and M. Dalby, Nanotopographical Control of Stem Cell Differentiation, *J. Tissue Eng.*, 2010, **1**, p 120623
51. W. Li, C. Laurencin, E. Caterson, R. Tuan, and F. Ko, Electrospun Nanofibrous Structure: A Novel Scaffold for Tissue Engineering, *J. Biomed. Mater. Res.*, 2002, **60**, p 613-621
52. A. Fomin, A. Steinhauer, V. Lyasnikov, S. Wenig, and A. Zakharevich, Nanocrystalline Structure of the Surface Layer of Plasma Sprayed Hydroxyapatite Coatings Obtained Upon Preliminary Induction Heat Treatment of Metal Base, *Tech. Phys. Lett.*, 2012, **38**, p 481-483
53. L. Sun, C. Berndt, K. Gross, and A. Kucek, Material Fundamentals and Clinical Performance of Plasma-Sprayed Hydroxyapatite Coatings, *J. Biomed. Mater. Res.*, 2001, **58**, p 570-592
54. M. Gottlander, ''On Hard Tissue Reactions to Hydroxyapatite-Coated Titanium Implants,'' PhD Thesis, Goteborgs Universitet, 1994
55. J. Jones, J. Lupori, J. Vansickles, and W. Gardner, A 5-Year Comparison of Hydroxyapatite-Coated Titanium Plasma-Sprayed Cylinder Dental Implants, *Oral Surg. Oral Med. Oral Pathol. Oral Radiol. Endod.*, 1998, **87**, p 649-652
56. T. Albrektsson, Hydroxyapatite-Coated Implants: A Case Against Their Use, *J. Oral Maxillofac. Surg.*, 1998, **56**, p 1312-1326
57. B. Chou and E. Chang, Microstructural Characterization of Plasma-Sprayed Hydroxyapatite-10 wt% ZrO_2 Composite Coating on Titanium, *Biomater*, 1999, **20**, p 1823-1832
58. T. Kasuga, M. Yoshida, A. Ikushima, M. Tuchiya, and H. Kusakari, Bioactivity of Zirconia-Toughened Glass-Ceramics, *J. Am. Ceram. Soc.*, 1992, **75**, p 1884-1888
59. S. Bauer, J. Park, J. Faltenbacher, S. Berger, K. von der Mark, and P. Schmuki, Size Selective Behavior of Mesenchymal Stem Cells on ZrO_2 and TiO_2 Nanotube Arrays, *Integr. Biol.*, 2009, **1**, p 525-532
60. Y. Xie, X. Liu, C. Ding, and P. Chu, Bioconductivity and Mechanical Properties of Plasma-Sprayed Dicalcium Silicate/Zirconia Composite Coating, *Mater. Sci. Eng. C*, 2005, **25**, p 509-515
61. T. Lee, C. Yang, E. Chang, and R. Tsai, Comparison of Plasma Sprayed Hydroxyapatite Coatings and Zirconia-Reinforced Hydroxyapatite Composite Coatings: In Vivo Study, *J. Biomed. Mater. Res. A*, 2004, **71A**, p 652-660
62. J. Si, J. Zhang, S. Liu, W. Zhang, D. Yu, X. Wang, L. Guo, and S. Shen, Characterization of a Micro-Roughened TiO_2/ZrO_2 Coating: Mechanical Properties and HBMSC Responses In Vitro, *Acta Biochim. Biophys. Sin.*, 2014, **46**, p 572-581
63. X. Zhao, G. Liu, H. Zheng, H. Cao, and X. Liu, Dose-Dependent Effects of CeO_2 on Microstructure and Antibacterial Property of Plasma-Sprayed TiO_2 Coatings for Orthopedic Application, *J. Thermal Spray Technol.*, 2015, **24**, p 401-409
64. A. Goh, M. Alshemary, M. Akram, M. Kadir, and R. Hussain, In-vitro Characterization of Antibacterial Bioactive Glass Containing Ceria, *Ceram. Int.*, 2014, **40**, p 729-737
65. M. Hassan, T. Amna, S. Al-Deyab, H. Kim, T. Oh, and M. Khil, Toxicity of Ce_2O_3/TiO_2 Composite Nanofibers Against *S. aureus* and *S. typhimurium*: A Novel Electrospun Material for Disinfection of Food Pathogens, *Colloids Surf.*, 2012, **415**, p 268-273
66. L. Hanch and J. Wilson, *An Introduction to Bioceramics*, World Scientific Publishing, Singapore, 1993
67. S. Tilmaz, M. Ipek, G. Celebi, and C. Bindal, The Effect of Bond Coat on Mechanical Properties of Plasma-Sprayed Al_2O_3 and Al_2O_3-13 wt% TiO_2 Coatings on AISI, 316L Stainless Steel, *Vacuum*, 2005, **77**, p 315-321
68. S. Sathish, M. Geetha, S. Aruna, N. Balaji, K. Rajam, and R. Asokamani, Studies on Plasma Sprayed Bi-Layered Ceramic Coating on Bio-Medical Ti-13Nb-13Zr Alloy, *Ceram. Int.*, 2011, **37**, p 1333-1339
69. F. Yildiz, A. Yetim, A. Alsaran, and A. Celik, Performance of Plasma Sprayed Al_2O_3 Coating in Bio-Simulated Environment, *Met. Sci. Heat Treat.*, 2014, **55**, p 504-508
70. M. Khalid, M. Mujahid, A. Khan, and R. Rawar, Dip Coating of Nano Hydroxyapatite on Titanium Alloy with Plasma Assisted G-Alumina Buffer Layer: A Novel Coating Approach, *J. Mater. Sci. Technol.*, 2013, **29**, p 557-564
71. K. Wapner, Implications of Metallic Corrosion in Total Knee Arthroplasty, *Clin. Orthop. Relat. Res.*, 1991, **271**, p 12-20
72. J. Black, Does Corrosion Matter?, *J. Bone Joint Surg.*, 1988, **70**, p 517-520
73. K. Hung, S. Lo, C. Shih, Y. Yang, H. Feng, and Y. Lin, Titanium Surface Modified by Hydroxyapatite Coating for Dental Implants, *Surf. Coat. Technol.*, 2013, **231**, p 337-345
74. C. Quek, K. Khor, and P. Cheang, Influence of Processing Parameters in the Plasma Spraying of Hydroxyapatite/Ti-6Al-4V Composite Coatings, *J. Mater. Process. Technol.*, 1999, **89-90**, p 550-555
75. J. Cizek, K. Khor, and Z. Prochazka, Influence of Spraying Conditions on Thermal and Velocity Properties of Plasma Sprayed Hydroxyapatite, *Mater. Sci. Eng. C*, 2007, **27**, p 340-344
76. S. Guessasma, G. Montavon, and C. Coddet, Velocity and Temperature Distributions of Alumina-Titania In-Flight Particles in the Atmospheric Plasma Spray Process, *Surf. Coat. Technol.*, 2005, **192**, p 70-76
77. Y. Tsui, C. Doyle, and T. Clyne, Plasma Sprayed Hydroxyapatite Coatings on Titanium Substrates Part 1: Mechanical Properties and Residual Stress Levels, *Biomaterials*, 1998, **19**, p 2015-2029
78. L. Sun, C. Berndt, and C. Grey, Phase, Structural and Microstructural Investigations of Plasma Sprayed Hydroxyapatite Coatings, *Mater. Sci. Eng. A*, 2003, **360**, p 70-84
79. S. Kweh, K. Khor, and P. Cheang, Plasma-Sprayed Hydroxyapatite (HA) Coatings with Flame-Spheroidized Feedstock: Microstructure and Mechanical Properties, *Biomaterials*, 2000, **21**, p 1223-1234
80. K. Gross, S. Saber-Samandari, and K. Heemann, Evaluation of Commercial Implants with Nanoindentation Defines Future Development Needs for Hydroxyapatite Coatings, *J. Biomed. Mater. Res. B*, 2010, **93**, p 1-8
81. X. Liu, S. Tao, and C. Ding, Bioactivity of Plasma Sprayed Dicalcium Silicate Coatings, *Biomaterials*, 2002, **23**, p 963-968
82. J. Yu, K. Li, X. Zheng, D. He, X. Ye, and M. Wang, In Vitro and In Vivo Evaluation of Zinc-Modified Ca-Si-Based Ceramic Coating for Bone Implants, *PLoS One*, 2013, **8**, p 1-10
83. A. El-Ghannam, P. Ducheyne, and I. Shapiro, Formation of Surface Reaction Products on Bioactive Glass and Their Effects on the Expression of the Osteoblastic Phenotype and the Deposition of Mineralized Extracellular Matrix, *Biomaterials*, 1997, **18**, p 295-303

84. I. Silver, J. Deas, and M. Ericinska, Interactions of Bioactive Glasses with Osteoblasts In Vitro: Effects of 45S5 Bioglass®, and 58S and 77S Bioactive Glasses on Metabolism, Intracellular Ion Concentrations and Cell Viability, *Biomaterials*, 2001, **22**, p 175-185
85. M. Yamaguchi, H. Oishi, and Y. Suketa, Stimulatory Effect of Zinc on Bone Formation in Tissue Culture, *Biochem. Pharmacol.*, 1987, **36**, p 4007-4012
86. H. Hsieh and J. Navia, Zinc Deficiency and Bone Formation in Guinea Pig Alveolar Implants, *J. Nutr.*, 1980, **110**, p 1581-1588
87. G. Oner, B. Bhaumick, and R. Bala, Effect of Zinc Deficiency on Serum Somatomedin Levels and Skeletal Growth in Young Rats, *Endocrinology*, 1984, **114**, p 1860-1863
88. G. Wang, Z. Lu, X. Liu, X. Zhou, C. Ding, and H. Zreiqat, Nanostructured Glass-Ceramic Coatings for Orthopaedic Applications, *J. R. Soc. Interface*, 2011, **8**, p 1192-1203
89. J. Sun, L. Wei, X. Liu, J. Li, B. Li, G. Wang, and F. Meng, Influences of Ionic Dissolution Products of Dicalcium Silicate Coating on Osteoblastic Proliferation, Differentiation and Gene Expression, *Acta Biomater.*, 2009, **5**, p 1284-1293
90. P. Valerio, M. Pereira, A. Goes, and M. Leite, The Effect of Ionic Products from Bioactive Glass Dissolution on Osteoblast Proliferation and Collagen Production, *Biomaterials*, 2004, **25**, p 2941-2948
91. H. Maleki-Ghaleh, M. Hafezi, M. Hadipour, A. Nadernezhad, E. Aghaie, Y. Behnamian, and N. Osman, Effect of Tricalcium Magnesium Silicate Coating on the Electrochemical and Biological Behavior of Ti-6Al-4V Alloys, *PLoS One*, 2015, **10**, p 1-14
92. M. Razavi, M. Fathi, O. Savabi, D. Vashaee, and L. Tayebi, Micro-arc Oxidation and Electrophoretic Deposition of Nano-Grain Merwinite ($Ca_3MgSi_2O_8$) Surface Coating on Magnesium Alloy as Biodegradable Metallic Implant, *Surf. Interface Anal.*, 2014, **46**, p 387-392
93. M. Razavi, M. Fathi, O. Savabi, B. Beni, D. Vashaee, and L. Tayebi, Nanostructured Merwinite Bioceramic Coating on Mg Alloy Deposited by Electrophoretic Deposition, *Ceram. Int.*, 2014, **40**, p 9473-9484
94. J. Ou, Y. Kang, Z. Huang, X. Chen, J. Wu, R. Xiao, and G. Yin, Preparation and In Vitro Bioactivity of Novel Merwinite Ceramic, *Biomed. Mater.*, 2008, **3**, p 015015
95. Y. Yang and E. Chang, Influence of Residual Stress on Bonding Strength and Fracture of Plasma-Sprayed Hydroxyapatite Coatings on Ti-6Al-4V Substrate, *Biomaterials*, 2001, **22**, p 1827-1836
96. D. Yi, C. Wu, B. Ma, H. Ji, X. Zheng, and J. Chang, Bioactive Bredigite Coating with Improved Bonding Strength, Rapid Apatite Mineralization and Excellent Cytocompatibility, *J. Biomater. Appl.*, 2014, **28**, p 1343-1353
97. Y. Xiao, L. Song, X. Liu, Y. Huang, T. Huang, Y. Wu, J. Chen, and F. Wu, Nanostructured Bioactive Glass-Ceramic Coatings Deposited by the Liquid Precursor Plasma Spraying Process, *Appl. Surf. Sci.*, 2011, **257**, p 1898-1905
98. H. Oonishi, L. Hench, J. Wilson, F. Sugihara, E. Tsuji, M. Matsuura, S. Kin, T. Yamamoto, and S. Mizokawa, Quantitative Comparison of Bone Growth Behavior in Granules of Bioglass® A-W Glass-Ceramic, and Hydroxyapatite, *J. Biomed. Mater.*, 2000, **51**, p 37-46
99. D. Garcia-Alonso, M. Parco, J. Stokes, and L. Looney, Low-Energy Plasma Spray (LEPS) Deposition of Hydroxyapatite/Poly-e-Caprolactone Biocomposite Coatings, *J. Thermal Spray Technol.*, 2012, **21**, p 132-143
100. K. Gross and C. Berndt, Thermal Processing of Hydroxyapatite for Coating Production, *J. Biomed. Mater. Res. A*, 1998, **39**, p 580-587
101. S. Radin and P. Ducheyne, Plasma Spraying Induced Changes of Calcium Phosphate Ceramic Characteristics and the Effect on In Vitro Stability, *J. Mater. Sci. Mater. Med.*, 1992, **3**, p 33-42
102. R. LeGeros, Biodegredation and Bioresorption of Calcium Phosphate Ceramics, *Clin. Mater.*, 1993, **14**, p 65-68
103. H. Maleki-Ghaleh, V. Khalili, J. Khalil-Allafi, and M. Javidi, Hydroxyapatite coating on NiTi Shape Memory Alloy by Electrophoretic Deposition Process, *Surf. Coat. Technol.*, 2012, **208**, p 57-63
104. P. Ducheyne, S. Radin, and L. King, The Effect of Calcium Phosphate Ceramic Composition and Structure on In Vitro Behavior. 1. Dissolution, *J. Biomed. Mater. Res.*, 1993, **27**, p 25-34
105. W. Xue, S. Tao, X. Liu, X. Zheng, and C. Ding, In Vivo Evaluation of Plasma Sprayed Hydroxyapatite Coatings Having Different Crystallinity, *Biomaterials*, 2004, **25**, p 415-421
106. K. Gross, B. Ben-Nissan, W. Walsh, and E. Swarts, Analysis of Retrieved Hydroxyapatite Coated Orthopaedic Implants, *Thermal spray: Meeting the challenges of the 21st century*, Nice, ASM International, 1998, pp. 1133-1138
107. A. Dey, In Vitro Dissolution, Microstructural and Mechanical Characterizations of Microplasma-Sprayed Hydroxyapatite Coating, *Appl. Ceram. Technol.*, 2014, **11**, p 65-82
108. A. Dey, A. Mukhopadhyay, S. Gangadharan, M. Sinha, and D. Basu, Characterization of Microplasma Sprayed Hydroxyapatite Coating, *J. Thermal Spray Technol.*, 2009, **18**, p 578-592
109. Y. Tsui, C. Doyle, and T.W. Clyne, Plasma Sprayed Hydroxyapatite Coatings on Titanium Substrates. Part 2: Optimisation of Coating Properties, *Biomaterials*, 1998, **19**, p 2031-2043
110. M. Morks and A. Kobayash, Effect of Gun Current on the Microstructure and Crystallinity of Plasma Sprayed Hydroxyapatite, *Appl. Surf. Sci.*, 2007, **253**, p 7136-7142
111. R. Heimann, Thermal Spraying Biomaterials, *Surf. Coat. Technol.*, 2006, **201**, p 2012-2019
112. A. Dey, S. Nandi, B. Kundu, C. Kumar, P. Mukherjee, S. Roy, A.K. Mukhopadhyay, M. Sinha, and D. Basu, Evaluation of Hydroxyapatite and b-Tri Calcium Phosphate Microplasma Spray Coated Pin Intra-Medullary for Bone Repair in a Rabbit Model, *Ceram. Int.*, 2011, **37**, p 1377-1391
113. A. Dey and K. Mukhopadhyay, Fracture Toughness of Microplasma-Sprayed Hydroxyapatite Coating by Nanoindentation, *Int. J. Appl. Ceram. Technol.*, 2011, **8**, p 572-590
114. H. Li, K. Khor, and P. Cheang, Young's Modulus and Fracture Toughness Determination of High Velocity Oxy-Fuel-Sprayed Bioceramic Coatings, *Surf. Coat. Technol.*, 2002, **155**, p 21-32
115. I. Demnati, M. Parco, D. Grossin, I. Fagoaga, C. Drouet, G. Barykin, C. Combes, I. Braceras, S. Goncalves, and C. Rey, Hydroxyapatite Coating on Titanium by a Low Energy Plasma Spraying Mini-Gun, *Surf. Coat. Technol.*, 2012, **206**, p 2346-2353
116. G. Wolinne, C. Harnisch, E. Heripre, S. Ruch, A. Salito, M. Jeandin, and L. Corte, Mechanical Study of Novel VPS-Titanium Coating on Polyethylene Substrates, *J. Thermal Spray Technol.*, 2014, **24**, p 206-214
117. S. Yugeswaran, C. Yoganand, A. Kobayashi, and K. Paraskevopoulos, Mechanical Properties, Electrochemical Corrosion and In Vitro Bioactivity of Yttria Stabilized Zirconia Reinforced Hydroxyapatite Coatings Prepared by Gas Tunnel Type Plasma Spraying, *J. Mech. Behav. Biomed. Mater.*, 2012, **9**, p 22-33
118. M. Roy, A. Bandyopadhyay, and S. Bose, Induction Plasma Sprayed Nano Hydroxyapatite Coatings on Titanium for Orthopaedic and Dental Implants, *Surf. Coat. Technol.*, 2011, **205**, p 2785-2792
119. K. Gross, C. Berndt, and H. Herman, Amorphous Phase Formation in Plasma-Sprayed Hydroxyapatite Coatings, *J. Biomed. Mater. Res.*, 1998, **39**, p 407-414
120. J. Weng, X. Liu, X. Li, and X. Zhang, Intrinsic Factors of Apatite Influencing Its Amorphization During Plasma-Spray Coating, *Biomaterials*, 1995, **16**, p 39-44
121. C. Yang and T. Lui, Effect of Crystallization on the Bonding Strength and Failures of Plasma-Sprayed Hydroxyapatite, *Mater. Trans.*, 2007, **48**, p 211-218
122. V. Amigo, M. Salvador, F. Romero, C. Solves, and J. Moreno, Microstructural Evolution of Ti-6Al-4V During the Sintering of Microspheres of Ti for Orthopedic Implants, *J. Mater. Process. Technol.*, 2003, **141**, p 117-122
123. J. Song, Y. Liu, Y. Zhang, and L. Jiao, Mechanical Properties of Hydroxyapatite Ceramics Sintered from Powders with Different Morphologies, *Mater. Sci. Eng. A*, 2011, **528**, p 5421-5427

124. J. Wang and L. Shaw, Nanocrystalline Hydroxyapatite with Simultaneous Enhancements in Hardness and Toughness, *Biomaterials*, 2009, **30**, p 6565-6572
125. J. Wang and L. Shaw, Morphology-Enhanced Low-Temperature Sintering of Nanocrystalline Hydroxyapatite, *Adv. Mater.*, 2007, **19**, p 2364-2369
126. H. Kim, Y. Kong, Y. Koh, H. Kim, H. Kim, and J. Ko, Pressureless Sintering and Mechanical and Biological Properties of Fluor-Hydroxyapatite Composites with Zirconia, *J. Am. Ceram. Soc.*, 2003, **86**, p 2019-2026
127. N. Ohtsu, Y. Nakamura, and S. Semboshi, Thin Hydroxyapatite Coating on Titanium Fabricated by Chemical Coating Process Using Calcium Phosphate Slurry, *Surf. Coat. Technol.*, 2012, **206**, p 2616-2621
128. N. Ohtsu, M. Hirano, and H. Arai, Response of Osteoblast-Like MC3T3-E1 Cells on Bioactive Titanium Fabricated by a Chemical Treatment Process Using a Calcium Phosphate Slurry, *J. Biomed. Mater. Res. A*, 2014, **102A**, p 3838-3845
129. N. Ohtsu, T. Takahara, M. Hirano, and H. Arai, Effect of Treatment Temperature on the Biocompatibility and Mechanical Strength of Hydroxyapatite Coating Formed on Titanium Using Calcium Phosphate Slurry, *Surf. Coat. Technol.*, 2014, **239**, p 185-190
130. I. Mobasherpour, M. Hashjin, and S. Toosi, Effect of the Addition ZrO_2-Al_2O_3 on Nanocrystalline Hydroxyapatite Bending Strength and Fracture Toughness, *Ceram. Int.*, 2009, **35**, p 1569-1574
131. S. Salehi and M. Fathi, Fabrication and Characterization of Sol-Gel Derived Hydroxyapatite/Zirconia Composite Nanopowders with Various Yttria Contents, *Ceram. Int.*, 2010, **36**, p 1659-1667
132. K. Pardun, L. Treccani, E. Volkmann, P. Streckbein, C. Heiss, G. Destri, G. Merletta, and K. Rezwan, Mixed Zirconia Calcium phosphate Coatings for Dental Implants: Tailoring Coating Stability and Bioactivity Potential, *Mater. Sci. Eng. C*, 2015, **48**, p 337-346
133. K. Pardun, L. Treccani, E. Volkmann, G. Destri, G. Merletta, P. Streckbein, C. Heiss, and K. Rezwan, Characterization of Wet Powder-Sprayed Zirconia/Calcium Phosphate Coating for Dental Implants, *Clin. Implant Dent. Relat. Res.*, 2015, **17**, p 186-198
134. L. Wang, X. Wang, C. Yu, and Y. Zhao, Effect of Titanium Addition on Thermal Stability of Hydroxyapatite/Zirconia Nanocomposite, *Sci. Sint.*, 2015, **47**, p 107-112
135. R. Sultana, J. Yang, and X. Hu, Deposition of Micro-Porous Hydroxyapatite/Tri-Calcium Phosphate Coating on Zirconia-Based Substrate, *J. Am. Ceram. Soc.*, 2012, **94**, p 1212-1215
136. S. Miao, K. Cheng, W. Weng, P. Du, G. Han, W. Yan, and S. Zhang, Fabrication and Evaluation of Zn Containing Fluoridated Hydroxyapatite Layer with Zn Release Ability, *Acta Biomater.*, 2008, **4**, p 441-446
137. A. Ito, M. Otsuka, H. Kawamura, M. Ikeuchi, H. Ohgushi, Y. Sogo, and N. Ichinose, Zinc-Containing Tricalcium Phosphate and Related Materials for Promoting Bone Formation, *Curr. Appl. Phys.*, 2005, **5**, p 402-406
138. M. Yamaguchi and R. Yamaguchi, Action of Zinc on Bone Metabolism in Rats: Increases in Alkaline Phosphatase Activity and DNA Content, *Biochem. Pharma*, 1986, **35**, p 773-777
139. V. Stanic, S. Dimitrijevic, J. Stankovic, M. Mitric, B. Jokic, B. Plecas, and S. Raicevic, Synthesis, Characterization and Antimicrobial Activity of Copper and Zinc-Doped Hydroxyapatite Nanopowders, *Appl. Surf. Sci.*, 2010, **256**, p 6083-6089
140. F. Bir, H. Khireddine, A. Touati, D. Sidane, S. Yala, and H. Oudadesse, Electrochemical Depositions of Fluorohydroxyapatite Doped by Cu^{2+}, Zn^{2+}, Ag^{+} on stainless steel substrates, *Appl. Surf. Sci.*, 2012, **258**, p 7021-7030
141. H. Kim, Y. Noh, Y. Koh, and H. Kim, Enhanced Performance of Fluorine Substituted Hydroxyapatite Composites for Hard Tissue Engineering, *J. Mater. Sci. Mater. Med.*, 2003, **14**, p 899-904
142. I. Uysal, F. Severcan, A. Tezcaner, and Z. Evis, Co-Doping of Hydroxyapatite with Zinc and Fluoride Improves Mechanical and Biological Properties of Hydroxyapatite, *Prog. Nat. Sci. Mat. Int.*, 2014, **24**, p 340-349
143. H. Demirkiran, Y. Hu, L. Zuin, N. Appathurai, and P. Aswath, XANES Analysis of Calcium and Sodium Phosphates and Silicates and Hydroxyapatite-Bioglass®45S5 Co-Sintered Bioceramics, *Mater. Sci. Eng. C*, 2011, **C31**, p 134-143
144. X. Chatzistavrou, E. Kontonasaki, K. Chrissafis, T. Zorba, P. Koidis, and K. Paraskevopoulos, Surface and Bulk Contributions in the Crystallization Process of a Bioactive Glass, *Key Eng. Mater.*, 2006, **309-311**, p 313-316
145. S. Radin and P. Ducheyne, Effect of Bioactive Ceramic Composition and Structure on In Vitro Behavior. III. Porous Versus Dense Ceramics, *J. Biomed. Mater. Res.*, 1994, **28**, p 1303-1309
146. W. Suchanek, M. Yashima, M. Kakihana, and M. Yoshimura, Hydroxyapatite Ceramics with Selected Sintering Additives, *Biomaterials*, 1997, **18**, p 923-933
147. D. Tancred, A. Carr, and B. McCormack, The Sintering and Mechanical Behaviour of Hydroxyapatite with Bioglass Additions, *J. Mater. Sci. Mater. Med.*, 2001, **12**, p 81-93
148. O. Filho, G. LaTorre, and L. Hench, Effect of Crystallization on Apatite-Layer Formation of Bioactive Glass 45S5, *J. Biomed. Mater. Res.*, 1996, **30**, p 509-514
149. P. Li, F. Zhang, and T. Kokubo, The Effect of Residual Glassy Phase in a Bioactive Glass Ceramic on the Formation of Its Surface Apatite Layer In Vitro, *J. Mater. Sci. Mater. Med.*, 1992, **3**, p 452-456
150. D. Bellucci, V. Cannillo, and A. Sola, Calcium and Potassium Addition to Facilitate the Sintering of Bioactive Glasses, *Mater. Lett.*, 2011, **65**, p 1825-1827
151. Q. Chen, I. Thompson, and A. Boccaccini, 45S5 Bioglass®-Derived Glass-Ceramic Scaffolds for Bone Tissue Engineering, *Biomaterials*, 2006, **30**, p 2414-2425
152. D. Bellucci, A. Sola, M. Gazzarri, F. Chiellini, and V. Cannillo, A New Hydroxyapatite-Based Biocomposite for Bone Replacement, *Mater. Sci. Eng. C*, 2013, **33**, p 1091-1101
153. K. Xie, L. Zhang, X. Yang, X. Wang, G. Yang, L. Zhang, H. Shao, Y. He, J. Fu, and Z. Gou, Preparation and Characterization of Low Temperature Heat-Treated 45S5 Bioactive Glass-Ceramic Analogues, *Biomed. Glasses*, 2015, **1**, p 80-92
154. A. Kirsten, A. Hausmann, M. Weber, J. Fischer, and H. Fischer, Bioactive and Thermally Compatible Glass Coating on Zirconia Dental Implants, *J. Dent. Res.*, 2015, **94**, p 297-303
155. R. Depprich, H. Zipprich, M. Ommerborn, C. Naujoks, H. Wiesmann, S. Kiattavorncharoen, H. Lauer, U. Meyer, N. Kübler, and J. Handschel, Osseointegration of Zirconia Implants Compared with Titanium: An In Vivo Study, *Head Face Med.*, 2008, **4**, p 30
156. H. Wenz, J. Bartsch, S. Wolfart, and M. Kern, Osseointegration and Clinical Success of Zirconia Dental Implants: A Systematic Review, *Int. J. Prosthodont.*, 2008, **21**, p 27-36
157. J. Gomez-Vega, E. Saiz, and A. Tomsia, Glass-Based Coatings for Titanium Implant Alloys, *J. Biomed. Mater. Res.*, 1999, **20**, p 1247-1253
158. M. Ferraris, E. Verné, P. Appendino, C. Moisescu, A. Krajewski, A. Ravaglioli, and A. Piancastelli, Coatings on Zirconia For Medical Applications, *Biomaterials*, 2000, **21**, p 765-773
159. J. Fischer, B. Stawarczyk, M. Tomic, J. Strub, and C. Hämmerle, Effect of Thermal Misfit Between Different Veneering Ceramics and Zirconia Frameworks on In Vitro Fracture Load of Single Crowns, *Dent. Mater. J.*, 2007, **26**, p 766-772
160. J. Lee, K. Hong, H. Baek, J. Seo, K. Lee, H. Ryu, and H. Lee, In Vivo Evaluation of CaO-SiO_2-P_2O_5-B_2O_3 Glass-Ceramics Coating on Steinman Pins, *Artif. Org.*, 2013, **37**, p 656-662
161. J. Lee, H. Nam, H. Ryu, J. Seo, B. Chang, and C. Lee, Bioactive Ceramic Coating of Cancellous Screws Improves the Osseointegration in the Cancellous Bone, *J. Orthop. Sci.*, 2011, **16**, p 291-297
162. L. Zhao, K. Lin, M. Zhang, C. Xiong, Y. Bao, X. Pang, and J. Chang, The Influences of Poly(Lactic-co-glycolic Acid) (PLGA) Coating on the Biodegradability, Bioactivity, and Biocompatibility of Calcium Silicate Bioceramics, *J. Mater. Sci.*, 2011, **46**, p 4986-4993

163. J. Middleton and A. Tipton, Synthetic Biodegradable Polymers as Orthopedic Devices, *Biomaterials*, 2000, **21**, p 2335-2346
164. Y. Huang, M. Connell, Y. Park, D. Mooney, and K. Rice, Fabrication and In Vitro Testing of Polymeric Delivery System for Condensed DNA, *J. Biomed. Mater. Res. A*, 2003, **67A**, p 1384-1392
165. F. Baino and C. Vitale-Brovarone, Feasibility Of Glass-Ceramic Coatings on Alumina Prosthetic Implants by Airbrush Spraying Method, *Ceram. Int.*, 2015, **41**, p 2150-2159
166. S. Murphy, D. Boyd, S. Moane, and M. Bennett, The Effect of Composition on Ion Release from Ca-Sr-Na-Zn-Si Glass Bone Grafts, *J. Mater. Sci. Mater. Med.*, 2009, **20**, p 2207-2214
167. A. Ito, H. Kawamura, M. Otsuka, M. Ikeuchi, H. Ohgushi, K. Ishikawa, K. Onuma, N. Kanzaki, Y. Sogo, and N. Ichinose, Zinc-Releasing Calcium Phosphate for Stimulating Bone Formation, *Mater. Sci. Eng. C*, 2002, **22**, p 21-25
168. D. Boyd, S. Murphy, M. Towler, A. Wren, and S. Hayakawa, Analysis of Gamma-Irradiated Synthetic Bone Grafts by Si-29 MAS-NMR Spectroscopy, Calorimetry and XRD, *J. Non Crystal Solids*, 2009, **355**, p 2285-2288
169. M. Looney, H. O'Shea, L. Gunn, D. Crowley, and D. Boyd, An Evaluation of the Processing Conditions, Structure, and Properties (Biaxial Flexural Strength and Antibacterial Efficacy) of Sintered Strontium-Zinc-Silicate Glass Ceramics, *J. Biomater. Appl.*, 2011, **27**, p 937-947
170. L. Esteban-Tejeda, L. Díaz, C. Prado, B. Cabal, and R. Torrecillas, Calcium and Zinc Containing Bactericidal Glass Coatings for Biomedical Metallic Substrates, *Int. J. Mol. Sci.*, 2014, **15**, p 13030-13044
171. I. Mutlu, Sinter-Coating Method for the Production of TiN-Coated Titanium Foam for Biomedical Implant Applications, *Surf. Coat. Technol.*, 2013, **232**, p 396-402
172. S. Piscaneca, L. Ciacchib, E. Vessellic, G. Comellic, O. Sbaizeroa, S. Meriania, and A. De Vita, Bioactivity of TiN-Coated Titanium Implants, *Acta Mater.*, 2004, **52**, p 1237-1245
173. W. Kim and H. Choe, Effects of TiN Coating on the Corrosion of Nanostructured Ti-30Ta-xZr Alloys for Dental Implants, *Appl. Surf. Sci.*, 2012, **258**, p 1929-1934
174. C. Liu and Q. Matthews, Tribological and Electrochemical Performance of PVD TiN Coatings on the Femoral Head of Ti-6Al-4V Artificial Hip Joints, *Surf. Coat. Technol.*, 2003, **163-164**, p 597-604
175. A. Zhecheva, W. Sha, S. Malinov, and A. Long, Enhancing the Microstructure and Properties of Titanium Alloys Through Nitriding and Other Surface Engineering Methods, *Surf. Coat. Technol.*, 2005, **200**, p 2192-2207
176. T. Sundararajan, U. KamachiMudali, K. Nair, S. Rajeswari, and M. Subbaiyan, In Vitro Corrosion Evaluation of Nitrogen Ion Implanted Titanium in Simulated Body Fluid, *Mater. Corros.*, 1999, **50**, p 344-349
177. I. Hung, W. Shih, M. Hon, and M. Wang, The Properties of Sintered Calcium Phosphate with (Ca)/(P) = 1.50, *Int. J. Mol. Sci.*, 2012, **13**, p 13569-13586
178. D. Mondal, L. Nguyen, I. Oh, and B. Lee, Microstructure and Biocompatibility of Composite Biomaterials Fabricated from Titanium and Tricalcium Phosphate by Spark Plasma Sintering, *J. Biomed. Mater. Res. A*, 2013, **101A**, p 1489-1501
179. Y. Liu, J. Huang, and H. Li, Synthesis of Hydroxyapatite-Reduced Graphite Oxide Nanocomposites for Biomedical Applications: Oriented Nucleation and Epitaxial Growth of Hydroxyapatite, *J. Mater. Chem. B*, 2013, **1**, p 1826-1834
180. E. Fernandez-Garcia, J. Guillem-Marti, C. Gutierrez-Gonzalez, A. Fernandez, M. Ginebra, and S. Lopez-Esteban, Osteoblastic Cell Response to Spark Plasma-Sintered Zirconia/Titanium Cermets, *J. Biomater. Appl.*, 2015, **29**, p 813-823
181. A. Kolk, J. Handschel, W. Drescher, D. Rothamel, F. Kloss, M. Blessmann, M. Heiland, K. Wolff, and R. Smeets, Current Trends and Future Perspectives of Bone Substitute Materials—From Space Holders to Innovative Biomaterials, *J. Craniomaxillofac. Surg.*, 2012, **40**, p 706-718
182. P. Manicone, P.R. Iommetti, and L. Raffaelli, An Overview of Zirconia Ceramics: Basic Properties and Clinical Applications, *J. Dent.*, 2007, **35**, p 819-826
183. J. Chevalier and L. Gremillard, Ceramics for Medical Applications: A Picture for the Next 20 Years, *J. Eur. Ceram. Soc.*, 2009, **29**, p 1245-1255
184. M. Hisbergues, S. Vendeville, and P. Vendeville, Review Zirconia: Established Facts and Perspectives for a Biomaterial in Dental Implantology, *J. Biomed. Mater. Res. B*, 2009, **88**, p 519-529
185. K. Lin and C. Lin, Reaction Between Titanium and Zirconia Powders During Sintering at 1500 C, *J. Am. Ceram. Soc.*, 2007, **90**, p 2220-2225
186. R. Domagala, S. Lyon, and R. Ruh, The Pseudobinary Ti-ZrO_2, *J. Am. Ceram. Soc.*, 1973, **56**, p 584-587